Chemistry
A European
Journal

Chemistry Europe
European Chemical Societies Publishing

Accepted Article

Title: Roles of Oxygen-Containing Functional Groups in Carbon for Electrocatalytic Two-Electron Oxygen Reduction Reaction

Authors: Guoqiang Zhao, Tianci Chen, Aidong Tang, and Huaming Yang

To be cited as: *Chem. Eur. J.* **2024**, e202304065

Link to VoR: https://doi.org/10.1002/chem.202304065

WILEY VCH

WILEY-VCH

Roles of Oxygen-Containing Functional Groups in Carbon for Electrocatalytic Two-Electron Oxygen Reduction Reaction

Guoqiang Zhao,[+] *Tianci Chen,*[+] *Aidong Tang,* Huaming Yang**

Prof. G. Zhao, T. Chen, Prof. A. Tang, Prof. H. Yang
Engineering Research Center of Nano-Geomaterials of Ministry of Education
China University of Geosciences, Wuhan, 430074, China
E-mail: tangaidong@cug.edu.cn (A. Tang); hm.yang@cug.edu.cn (H. Yang)

Prof. G. Zhao, T. Chen, Prof. A. Tang, Prof. H. Yang
Faculty of Materials Science and Chemistry
China University of Geosciences, Wuhan, 430074, China

Prof. G. Zhao, Prof. A. Tang, Prof. H. Yang
Laboratory of Advanced Mineral Materials
China University of Geosciences, Wuhan, 430074, China

Prof. A. Tang
College of Chemistry and Chemical Engineering
Central South University, Changsha 410083, China

Prof. H. Yang
Hunan Key Laboratory of Mineral Materials and Application
School of Minerals Processing and Bioengineering
Central South University, Changsha 410083, China

[+] These authors contribute equally to this work.

Keywords: oxygen-containing functional groups, carbon, oxygen reduction reaction, selectivity, structure-function relationship

Abstract

Recent years have witnessed great research interests in developing high-performance electrocatalysts for the two-electron ($2e^-$) oxygen reduction reaction (ORR) that enables the sustainable and flexible synthesis of H_2O_2. Carbon-based electrocatalysts exhibit attractive catalytic performance for the $2e^-$ ORR, where oxygen-containing functional groups (OFGs) play a decisive role. However, current

understanding is far from adequate, and the contribution of OFGs to the catalytic performance remains controversial. Therefore, a critical overview on OFGs in carbon-based electrocatalysts toward the $2e^-$ ORR is highly desirable. Herein, we go over the methods for constructing OFGs in carbon including chemical oxidation, electrochemical oxidation, and precursor inheritance. Then we review the roles of OFGs in activating carbon toward the $2e^-$ ORR, focusing on the intrinsic activity of different OFGs and the interplay between OFGs and metal species or defects. At last, we discuss the reasons for inconsistencies among different studies, and personal perspectives on the future development in this field are provided. The results provide insights into the origin of high catalytic activity and selectivity of carbon-based electrocatalysts toward the $2e^-$ ORR and would provide theoretical foundations for the future development in this field.

1 Introduction

Hydrogen peroxide (H_2O_2) is one of the most important chemicals and has been widely used as oxidizers, antiseptics, or bleaching agents in a variety of industries.[1-4] The global annual H_2O_2 demand now is estimated to be 4.5 million tons and is increasing continually.[5-6] To date, while the vast majority of industrial H_2O_2 is produced via the energy-demanding and waste-intensive anthraquinone process,[7-8] electrochemical synthesis of H_2O_2 from the two-electron ($2e^-$) oxygen reduction reaction (ORR) has achieved increasing attention as a green, mild, and flexible approach to the decentralized H_2O_2 production.[9-13] Advanced electrocatalysts with high activity and selectivity toward the $2e^-$ ORR are central to the efficient H_2O_2

electrochemical production because oxygen can also be reduced to H_2O via the four-electron ($4e^-$) ORR that will decrease the Faradaic efficiency.[14-18] Recently, numerous carbon-based materials such as HNO_3-treated carbon nanotubes (CNTs),[19] reduced graphene oxide (rGO),[20] and Co_1-NG(O)[21] have shown significant potential regarding the electrochemical synthesis of H_2O_2 due to their competitive performance and low cost.[22-27] These carbon-based catalysts are usually enriched with oxygen, and oxygen-containing functional groups (OFGs) have been demonstrated to play a critical role in achieving high activity and selectivity toward the $2e^-$ ORR.[28-31] In general, the sp^2 or sp^3 hybridized carbon atoms generally possess low electrocatalytic performance due to their weak electrochemical adsorption ability, and OFGs such as carboxyl (–COOH), carbonyl (–C=O), hydroxyl (–OH), epoxide (–C–O–C) groups can modulate the local electronic structures efficiently,[32-35] thereby creating adsorption sites for the reaction. Meanwhile, the oxygen atoms in OFGs possess lone pairs and thus can act as nucleophilic Lewis base sites in electrochemical reactions.[36] In addition, OFGs may also contribute to the overall reaction by tuning the physicochemical properties of the catalyst such as the wettability.[37-40] Therefore, it is quite necessary to review the chemistry of OFGs for the further development of high-performance oxygen-rich carbon-based electrocatalysts toward the $2e^-$ ORR.

There are two basic types of bondings between carbon and oxygen atoms including the carbon–oxygen single bond (C–O) and carbon–oxygen double bond (C=O). The bond length for typical C–O is in the range of 1.36~1.43 Å,[41] and the value for

C=O is 1.23 Å in carbonyl-related OFGs.[42] Therefore, OFGs can be classified as C–O containing groups and C=O containing groups. As illustrated in **Figure 1**, hydroxyl and epoxide groups contain only C–O bond, and carbonyl and quinone groups possess only C=O bond. Also, there are OFGs containing both C–O and C=O bonds such as carboxyl, ester, anhydride, and aldehyde groups. The differences between the physicochemical properties of these OFGs, in particular OFGs with the same carbon–oxygen bond, are usually not obvious, and thus it is a rather big challenge to distinguish different OFGs. From a chemical point of view, some OFGs such as hydroxyl and carboxyl groups are acidic, and their amounts can be evaluated by the acid-base titration method,[43-44] but it is quite challenging to distinguish different acidic groups using this method.[45] Temperature programmed desorption (TPD) is a popular method to evaluate OFGs, where different OFGs may decompose at varied temperatures under an inert atmosphere to release CO and CO_2. The types and amounts of OFGs can then be determined by deconvolving TPD spectra.[46] Data interpretations can be challenging because the OFG decomposition temperatures are determined by multiple factors including the experimental parameters and the texture of carbon materials, and the secondary reactions between elevated gases and the samples also make the results more complicated.[47] Nevertheless, some general principles still can be established. For example, carboxylic acids are the least stable groups, releasing CO_2 at low temperatures, and lactones also release CO_2 but at higher temperatures; carboxylic anhydrides release both CO_2 and CO; phenols, ethers, and carbonyls release CO at relatively high

temperatures.[47] X-ray photoelectron spectroscopy (XPS) is another frequently used method to determine OFGs based on the varied binding energies of carbon or oxygen in different chemical states. Typically, there could be sp^2 carbon, sp^3 carbon, C–O, C=O, COOH, and π-π* satellite in C1s XPS spectra in the order of binding energy from low to high. The situation for O1s XPS spectra is somewhat more complicated as the contributions from H_2O molecules are very difficult to avoid. Near-edge X-ray absorption fine structure (NEXAFS) spectra at the C K-edge and O K-edge provide more detailed information on orbital hybridizations, but lots of experience are required for appropriate data interpretations. In practice, the type and amount of OFGs in carbon-based materials can be collectively determined by multiple methods including XPS, NEXAFS, TPD, electrochemical methods, etc.

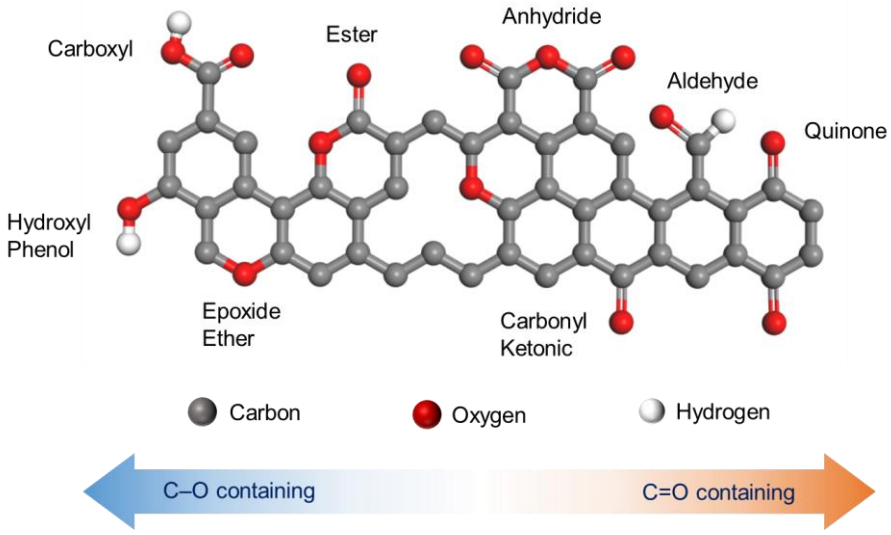

Figure 1. The structure model of typical OFGs in carbon-based materials.

It has been recognized that the $2e^-$ ORR activity of the catalyst is largely determined by the adsorption free energy of OOH* (ΔG_{OOH*}) on active sites, because OOH* is the only intermediate in the reaction. The generation of OOH* will be retarded when

the OOH* adsorption is too weak; in contrast, the overall reaction will be hindered by the desorption of OOH*, i.e. the protonation of *OOH, if the catalyst binds OOH* too strongly. Therefore, the $2e^-$ ORR activity of the catalyst shows a volcano relationship between the ΔG_{OOH*}, which is similar to the hydrogen evolution reaction.[48] **Figure 2**a displays the activities of some oxygen-rich carbon electrocatalysts with different OFGs as active sites together with several noble-metal-based catalysts. [19, 21, 30-31, 49-51] The activity is represented by the limiting potential U_L, which is defined as the lowest potential at which all the reaction steps are downhill in free energy, and the ΔG_{OOH*} on active sites is employed as the descriptor of the catalyst structure. The highest activity toward the $2e^-$ ORR is achieved at around 4.2 eV for ΔG_{OOH*}.[52] Meanwhile, the ΔG_{OOH*} also exerts significant influences on the selectivity of catalyst toward the ORR. Catalysts that bind OOH* strongly facilitate the break of the O–O bond, leading to the low $2e^-$ ORR selectivity. Moreover, ΔG_{OOH*} is not the sole factor that determines the reaction, and other factors, kinetic barrier for example,[48] also impact the reaction process to a large extent. As illustrated in Figure 2b, the kinetic barrier for OOH* protonation versus the dissociation is the decisive factor for the selectivity toward the $2e^-$ or $4e^-$ path of the ORR.[52-53] In carbon-based electrocatalysts, as shown in Figure 2c-d, OFGs including ether, carboxyl, and hydroxyl groups may readily modulate the ΔG_{OOH*} of active sites by tuning the local electronic structures. The ΔG_{OOH*} was increased from 3.6 eV to 4.72 eV as the charge increases, demonstrating a linear relationship between ΔG_{OOH*} and the charge state of the active carbon

atoms.[21, 54]

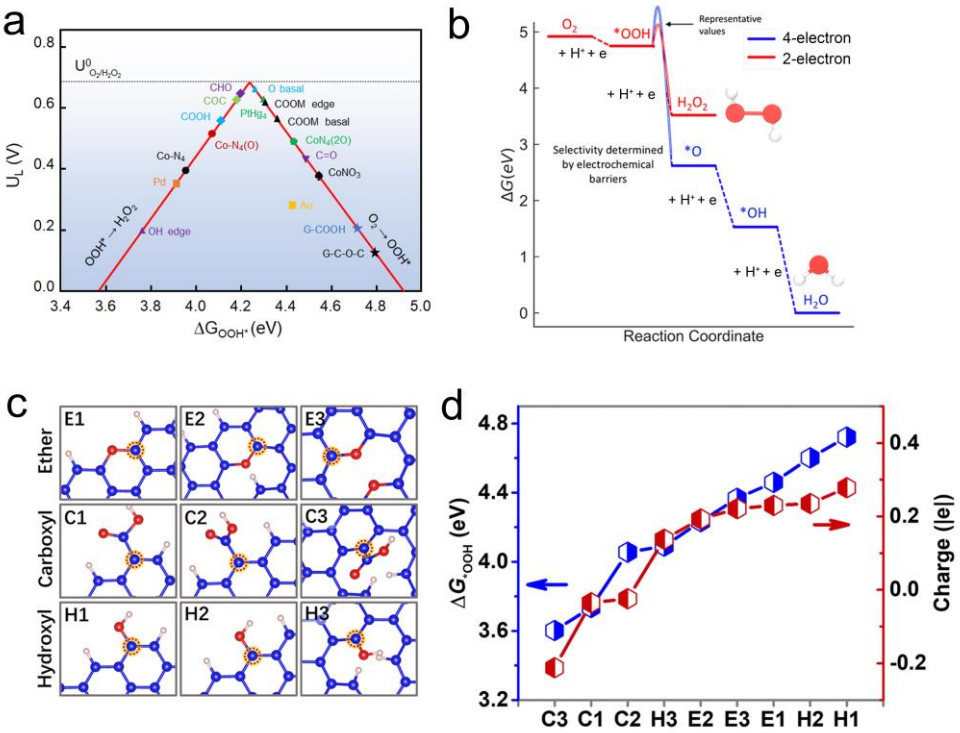

Figure 2. (a) The volcano plot for the 2e⁻ ORR with the limiting potential plotted as a function of the ΔG_{OOH*}. Data are obtained from references for ●[21], ▲[19], ▼[30], ■[31], ★[49], ♠[50], and ◆[51]. (b) The free energy diagram for the 4e⁻ and 2e⁻ ORR on Au(111) in blue and red, respectively. The energy barriers for OOH* to *O or H_2O_2 are illustrative. Reproduced with permission.[53] Copyright © 2018, American Chemical Society. (c) Carbon configurations with various OFGs at different positions, and the red dotted circles illustrate the active centers. (d) The ΔG_{OOH*} and charge states of the active carbon sites in Figure 2c. Reproduced with permission.[54] Copyright © 2022, The Royal Society of Chemistry.

To date, while extensive studies have demonstrated that OFGs are crucial to activating oxygen-rich carbon electrocatalysts toward the 2e⁻ ORR, systematic understandings on the role of OFGs in the reaction are not adequate. In particular, there is apparent inconsistency in the contributions of OFGs to the 2e⁻ ORR, and the reported roles of OFGs vary in different studies, as listed in **Table 1**. Therefore, it is highly desirable to provide a systematic summary on the preparation methods

for oxygen-rich carbon electrocatalysts and an in-depth discussion on the roles of OFGs in the 2e⁻ ORR. In this review, we first outline the common methods to constructing and regulating the OFGs in oxygen-rich carbon electrocatalysts, highlighting the differences between various methods. After that, the roles of specific OFGs in the 2e⁻ ORR are discussed with focus on their influences on the local electronic structures. At last, we provide our personal perspectives on the future development on the oxygen-rich carbon electrocatalysts for the 2e⁻ ORR.

Table 1. The reported roles of OFGs to the 2e⁻ ORR in different studies

Carbon	Method	Main OFGs	2e⁻ ORR selectivity	Remarks	Reference
CNT	12 M HNO_3 treatment at 80 °C for different time	both C–O and C=O containing groups	~90% in 0.4–0.65 V	The 2e⁻ ORR activity and selectivity were positively related to the oxygen content. Carbon atoms adjacent to several OFGs (carboxyl and epoxide) are the active sites.	[19]
	hydrothermal in 6 M KOH solution at 180 °C for 12h	C=O containing groups	~83% in 0.4–0.65 V		
	mix with PEO and carbonized at 600 °C under an Ar atmosphere	C–O containing groups	~87% in 0.4–0.65 V		
mesoporous carbon	thermal oxidation in air at 400 °C	hydroxyl groups	~90%	Carboxyl groups possess intrinsically high catalytic activity. Electrons are transferred from carboxyl groups to adjacent carbon, which enhances adsorption strength toward *OOH intermediate	[55]
	treating with 6 M HNO_3 solution at 60 °C for 12 h	carboxyl groups	~89%		
	hydrothermal in 6 M H_2O_2 solution at 180 °C for 12h	carboxyl groups	94%		
carbon black	calcination treatment at 200, 400, and 600°C	carboxyl and hydroxyl groups	50–60%	Carboxyl and epoxide groups promote the 2e⁻ ORR.	[37]

carbon black	annealing in air at 500 °C for different time	aldehyde, epoxide, and carbonyl	>94% in 0.4–0.7V	Epoxide and aldehyde groups contribute more to the H_2O_2 production	[51]
edge-oxygenated GNP[a]	treated with mild oxidants of CO_2	carbonyl-related groups	90–95% in 0.5–0.7 V	Carbonyl-related groups including quinone and carboxylic acid groups were more active than in-plane etheric rings.	[28]
	treated with diluted O_2	epoxide groups	83–88% in 0.5–0.7 V		
Co/N co-doped CNTs	two-step electrochemical oxidation and electrochemical reduction	more epoxide groups and carboxyl groups	>90% in 0.3–0.65V	Electrochemical reduction removes most of the carboxyl groups. The retaining stable epoxide groups tunes the electronic structure of Co centers.	[31]
GO[b]	treated with KBH_4 solution at 80 °C	hydroxyl groups	60–68%	Epoxide groups contribute to high selectivity toward the $2e^-$ ORR.	[56]
	treated with KOH solution at 140 °C for 2 h	epoxide groups	~100%		
multi-walled CNTs	modified Hummer's oxidation	ether-type oxygen groups	/	OFG is necessary for the ORR rather than the edge defects. Epoxide groups possess the best activity but are less favorable for O_2 adsorption, while carbonyl groups promote O_2 adsorption.	[57]
	H_2SO_4-catalyzed HNO_3 oxidation	carboxyl groups	/		

a: GNP—graphitic nanoplatelet; b: GO—graphene oxide.

2 Preparation methods for oxygen-rich carbon catalysts

Based on the materials formation mechanism, there are two primary methods to prepare oxygen-rich carbon catalysts. The first method starts from the existing carbon material, and OFGs can be introduced from the outside by

chemical/electrochemical oxidation, plasma treatment, etc.[35, 58-60] Here, OFGs are derived from additional precursors other than the carbon, which is like a mathematical addition operation. The other method starts with precursors, and OFGs are inherited from the same precursor of carbon. For example, OFG-enriched graphene can be obtained by partially reducing graphene oxide (GO), and oxygen-rich carbon can be prepared by calcining glucose and epoxy molecules.[56, 61-62]

2.1 Chemical oxidation

Chemical oxidation is a straightforward method with regard to introducing OFGs into carbon. Pristine carbon materials react with strong oxidants such as concentrated HNO_3 solution, H_2O_2 solution, and oxygen gas, where oxygen atoms can be introduced into different positions in carbon matrix, forming various types of OFGs.[63-64] Lu et al. synthesized oxidized carbon nanotubes (O-CNTs) by treating CNTs with concentrated HNO_3 solution at 80 ℃.[19] The deconvoluted O 1s X-ray photoelectron spectroscopy (XPS) spectra in **Figure 3**a demonstrate that the O-CNTs possess both C–O containing OFGs and C=O containing OFGs. The oxygen content of O-CNTs was increased with the treatment time, and a high oxygen content of 9% was achieved after 48 hours of the treatment. Interestingly, the activity and selectivity of O-CNTs toward the $2e^-$ ORR were found to be positively related to the oxygen content (Figure 3b-c). Besides, the $2e^-$ ORR selectivity of the O-CNTs was dramatically decreased after being treated under a 20% H_2/Ar atmosphere at 800 ℃ for 2h, which removed most of the OFGs, highlighting the crucial roles of OFGs toward the $2e^-$ ORR process. Moreover, carbon black and

acetylene black were oxidized via similar procedures, and the selectivity toward the 2e⁻ ORR was also enhanced, accordingly. This work demonstrated the universality of the concentrated HNO_3 oxidation method for constructing OFGs in carbon materials and highlighted the significance of OFGs in the 2e⁻ ORR.

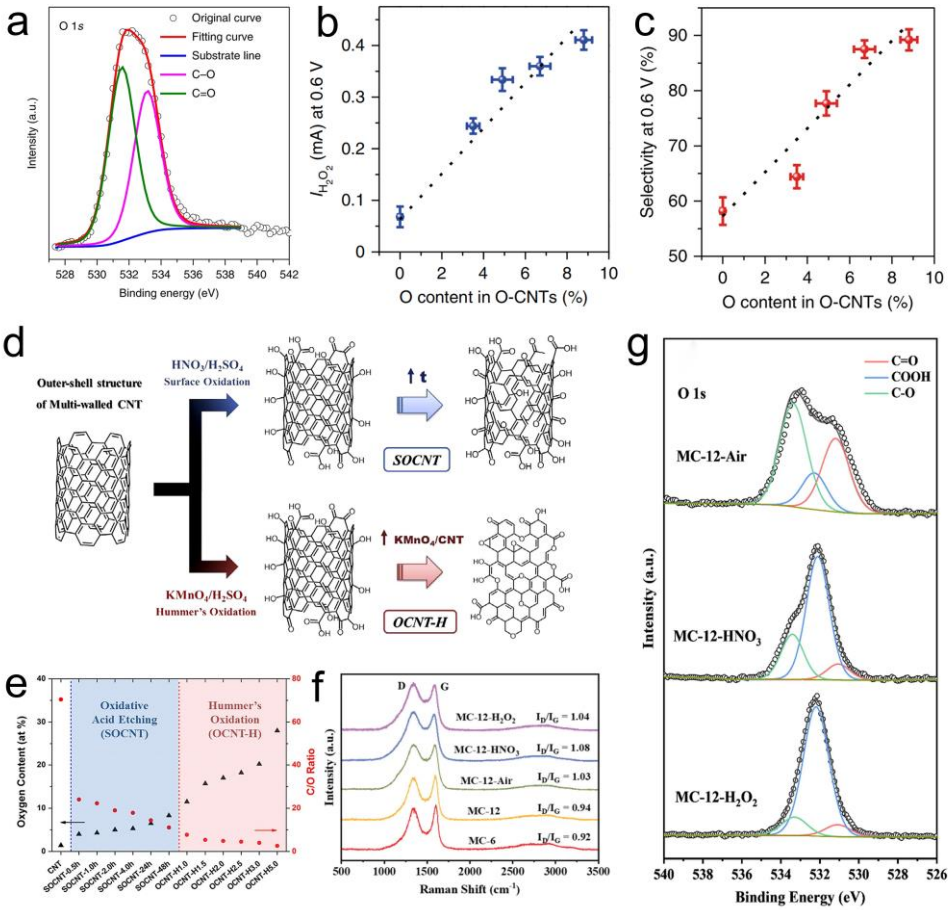

Figure 3. (a) Deconvoluted O 1s spectra of O-CNTs. (b, c) Plots of b) H_2O_2 current and c) 2e⁻ ORR selectivity at 0.6 V as a function of oxygen content of O-CNTs. Reproduced with permission.[19] Copyright © 2018, Springer Nature. (d) Illustration of the outer-shell structure of CNTs and the structural evolution of the O-CNTs during the Hummer's oxidation and the oxidative acid etching processes. (e) The evaluated oxygen contents and C/O ratios of the CNTs based on XPS results. Reproduced with permission.[57] Copyright © 2014, Elsevier. (f) Raman spectra and (g) O1s XPS spectra of the samples. Reproduced with permission.[55] Copyright © 2022, Elsevier.

The Hummer's method, which uses $KMnO_4$ and concentrated H_2SO_4 as the oxidants,

is commonly used for preparing GO and is also highly efficient with regard to introducing OFGs into carbon.[65-66] As illustrated in Figure 3d, Gentle et al. performed the oxidation of multi-walled CNTs (MWCNTs) via two different methods.[57] For one, MWCNTs were treated by surface oxidation using HNO_3/H_2SO_4 as the oxidants, introducing abundant carboxyl groups, and the obtained sample were denoted as SOCNTs. For another, a modified Hummer's oxidation method was employed, where the obtained OCNTs-H were unzipped through the longitudinal direction, and ether-type oxygen groups were the primary species when a high mass ratio of $KMnO_4$:CNT was used.[67] By varying the treatment time and the mass ratio of $KMnO_4$:CNT, the oxygen content of SOCNTs and OCNTs-H can be modulated, respectively. As demonstrated in Figure 3e, the Hummer's oxidation method was more effective than the oxidative acid etching with respect to achieving high oxygen content. On the other hand, excessive oxygen atoms will disturb the π-bond conjugated structures of graphite sheets, and thereby decrease the electronic conductivity.[68] Therefore, it is important to optimize the oxygen content to balance the electronic conductivity and the catalytic activity/selectivity. In another work,[69] MWCNTs were also treated with a modified Hummers method, and the optimized sample possessed abundant defects and OFGs in the surface of outer layers, while the inner layers remained intact. Such a unique structure ensures sufficient active sites and high electronic conductivity, simultaneously, providing an effective route to the compromise between activity and conductivity. In the meantime, it has been reported that Mn-based impurities may

exist in carbon materials due to the use of large amounts of permanganate oxidants in the Hummers oxidation treatment.[70] These metal impurities can play as additional active sites for the ORR, which should be carefully assessed or removed for a more precise evaluation on the catalytic role of OFGs.

Hydrothermal treatment is another method that is frequently employed to regulate OFGs of carbon-based materials. Bryan et al. reported that a hydrothermal treatment of MWCNTs introduced C=O containing OFGs such as ketonic and carboxyl groups.[38] These additional OFGs improved the hydrophilicity by facilitating the formation of hydrogen bonds with water and served as strong electron-withdrawing sites, thereby improving the electrochemical activity of MWCNTs toward the $2e^-$ ORR. While the total oxygen content remained relatively constant, the ratio of C=O to C–O containing species was improved at enhanced temperature, indicating a thermally-driven transformation from C−O containing groups to carboxyl/ketonic groups. Similar structure transformation between OFGs was also reported in a recent work.[55] In detail, mesoporous carbons (MC-12) were treated with chemical oxidation by 6 M HNO_3 solution at 60 ℃ for 12 h and with hydrothermal in 6 M H_2O_2 solution at 180 ℃ for 12h, and the obtained samples were denoted as MC-12-HNO_3 and MC-12-H_2O_2, respectively. Besides, MC-12-Air was prepared by thermal oxidation of MC-12 in air at 400 ℃. Figure 3f shows the Raman spectra of the samples, and the increased I_D/I_G value indicates the more defective carbon structures after the oxidation treatment. The O1s XPS spectra (Figure 3g) reveal that the hydroxyl group is dominating in MC-12-Air, while carboxyl groups are the primary

species in MC-12-HNO_3 and MC-12-H_2O_2. It was reported that carbon materials undergone a multistep oxygen functionalization mechanism in the presence of strong oxidants—carbonyl groups were first formed from mono-vacancies, followed by the transformation to hydroxyl groups and then carboxyl groups together with the enlargement of vacancies.[58] Therefore, the higher ratio of carboxyl groups in MC-12-H_2O_2 as compared with MC-12-HNO_3 was ascribed to the higher temperature that promoted the transformation from hydroxyl groups to carboxyl groups.[55] Meanwhile, it is worth noting that nitrogen-containing groups, in particular nitro groups can also be introduced;[71] however, it seems that this has been overlooked when using HNO_3 as the oxidant, constantly. This issue should not be ignored and deserves more attention in future works. Furthermore, the presence of hydrogen would significantly decrease the thermal stability of OFGs in HNO_3-treated MWCNTs.[72] Carboxylic groups were reduced to phenolic groups at 300 °C in a hydrogen atmosphere, but it was fail to remove all oxygen species even at a high temperature of 720 °C.[72] The varied thermal stability of different OFGs in different environment provide feasibilities for the regulation of OFGs in oxygen-rich carbon electrocatalysts.

10.1002/chem.202304065

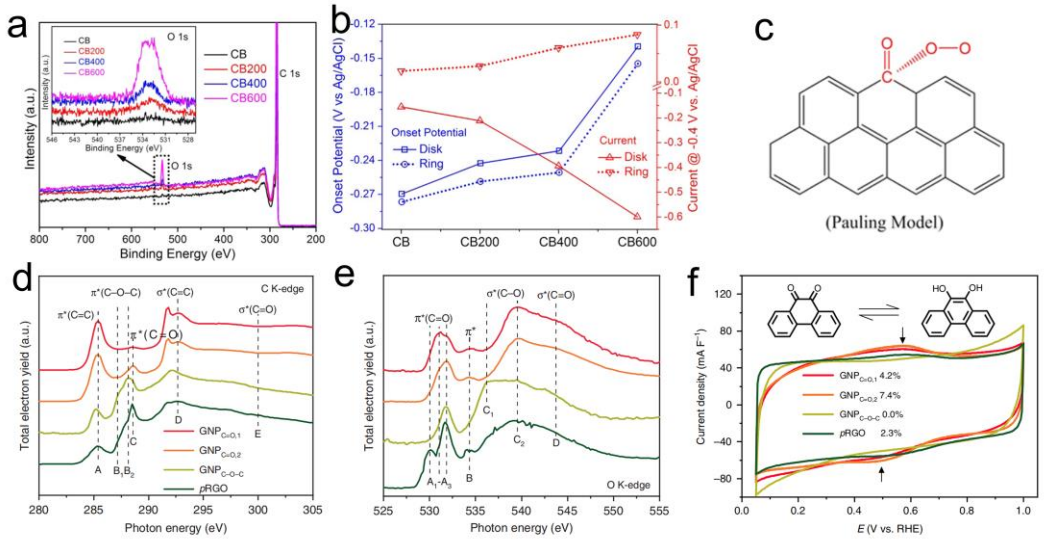

Figure 4. (a) XPS spectra of the samples, and the inset shows the O1s spectra. (b) The onset potential and the current at –0.4 V on the rotating ring-disk electrode (RRDE) for different catalysts in 0.1 M Na_2SO_4 solution. (c) The Pauling model of oxygen adsorption toward the $2e^-$ ORR. Reproduced with permission.[37] Copyright © 2019, American Chemical Society. (d-e) NEXAFS spectra of the sample at d) the C K-edge and e) the O K-edge. (f) The cyclic voltammetry in Ar-saturated 0.5 M H_2SO_4 at a scan rate of 50 mV s^{-1}, showing the quinone redox behavior. Reproduced with permission.[28] Copyright © 2020, The Authors.

In addition to liquid-phase oxidants, gas-phase oxidants such as oxygen and ozone are also frequently employed to oxidize carbon materials.[73-74] For instance, Park et al. constructed hydroxyl and carboxyl groups on the outer surface of single-walled CNTs (SWCNTs) using O_3 gas flow as the oxidant.[75] In another work, OFGs were introduced in carbon black (CB) by calcinating at 200, 400, and 600 °C in air, while CB was oxidized completely to CO_2 at 700 °C.[37] As shown in the XPS spectra in **Figure 4**a, the highest oxygen content is achieved at 600 °C, and the oxygen atom ratio is increased from the initial 1.17 ± 0.15% for the pristine CB to 4.08 ± 0.60% for CB600. The onset potentials and the ring current at –0.4 V of different catalysts are shown in Figure 4b, where CB600 exhibits the highest onset potential as well as

the highest ring current of 0.08 mA. The improved performance was attributed to the regulated O_2 adsorption mode due to the increased OFGs. To be specific, the carbon atoms in carbonyl and carboxyl groups possess net positive charges, which facilitate the adsorption of O_2 molecule via the end-on mode, i.e. the Pauling model (Figure 4c), that was kinetically favored by the $2e^-$ ORR.[76-77] Moreover, the additional carboxyl and hydroxyl groups also rendered the catalyst with hydrophilic surface that accelerates the diffusion of O_2 to active sites. These positive effects of OFGs promote the $2e^-$ ORR, collectively.

On the other hand, harsh oxidation conditions are usually required during the chemical oxidation processes to cleave the strong sp^2 C–C bonds to introduce OFGs, which makes the regulation of targeted OFGs less controllable. In this case, Han et al. developed a two-step gas-phase chemical oxidation method to construct specific OFGs in graphitic nanoplatelets (GNP).[28] Graphite powders were first crushed and exfoliated into nanosized particles by mechanochemical ball-milling, and then the exposed broken edges were reacted with mild oxidants. Carbonyl-related groups (quinone and carboxylic groups) and etheric rings were the major OFGs when CO_2 and dilute O_2 were used as the mild oxidants, respectively. In detail, the $GNP_{C=O,1}$ was prepared by ball-milling GNP with dry ice, and quinone groups were easily formed with an oxygen content of 10.5 at%. Providing the increased ball-milling time and the enhanced mass ratio of dry ice to graphite, the $GNP_{C=O,2}$ was obtained and the oxygen content was improved to 20.6 at% with carboxylic acid groups being the major species. When the dilute O_2 atmosphere was employed as the oxidant, the

obtained samples ($GNP_{C–O–C}$) were enriched with etheric rings. Figure 4d shows the near-edge X-ray absorption fine structure (NEXAFS) at the C K-edge of the samples, demonstrating unoccupied π* (peak A–C) and excited σ* (peak D, E) states. For the peak B, the peak B_1 at 287.2 eV and the peak B_2 at 288.2 eV are ascribed to the out-of-plane and the in-plane C–O bonding of epoxide groups (C–O–C), respectively. Therefore, the $GNP_{C–O–C}$ is composed of major in-plane epoxide and minor out-of-plane epoxide species. The peak C at around 288.6 eV is attributed to π*(C=O) and should be determined in combination with other characterizations. The XANES spectra at the O K-edge are shown in Figure 4e. The A_1 peak at 530.1 eV is derived from the π*(C=O) of organic carbonates, and is only found in the partially reduced graphene oxide (pRGO). Peak A_2 at 531.0 eV is ascribed to quinone groups, and the results indicate that quinone groups are the primary OFG for $GNP_{C=O,1}$, while the $GNP_{C=O,2}$ and pRGO also contain a few quinone groups. Meanwhile, the primary A_3 and C_2 peaks in $GNP_{C=O,2}$ and pRGO indicate they possess abundant carboxyl groups. Cyclic voltammetry (CV) was employed to further investigate the type of OFGs based on the redox couple of quinone groups (Figure 4f), and the quinone contents were estimated to be 4.2%, 7.4%, 0.0%, and 2.3% for $GNP_{C=O,1}$, $GNP_{C=O,2}$, $GNP_{C–O–C}$, and pRGO, respectively. Electrochemical performance revealed that quinone-enriched samples exhibit high selectivity and activity toward the $2e^-$ ORR, and the activity trends of different quinone groups were investigated using DFT calculations, which will be discussed in detail later.

2.2 Electrochemical oxidation

Similar to chemical oxidation, OFGs can be introduced into carbon matrix by electrochemical oxidation treatments.[78-80] Different from chemical oxidation, the electrochemical oxidation of carbon is usually accompanied by the formation of micropores, leading to the increased specific surface area.[81] Moreover, the electrochemical oxidation of carbon usually takes place in aqueous solution, and the nature of electrolyte exerts significant impacts on the oxidation degree. For example, Bauer et al. performed electrochemical anodic oxidation of carbon fibers in an alkaline NH_4HCO_3 aqueous solution (pH ≈ 8) and an acidic H_2SO_4 solution (pH ≈ 2) by a galvanostatic method.[82] The results revealed much higher oxidation degree in the acidic electrolyte than in the alkaline. It is interesting to notice that carbon can be oxidized at both the anode and the cathode sides in an electrochemical cell. As illustrated in the electrochemical cell in **Figure 5**a-b,[83] carbon nanofibers (CNFs) were dispersed in 5% H_2SO_4 solution and coated on electrode surface without binder, which were used as both the anode and the cathode. Electrochemical oxidation was performed under galvanostatic conditions at different potentials for 30 min. The XPS spectra showed the O/C atom ratio for the pristine CNFs (0.23) was increased after the electrochemical treatment. Counterintuitively, the O/C atom ratio of the CNF at the cathode (0.37) is higher than that at the anode (0.33). The authors proposed that the CNFs at the anode undergone merely the general electrochemical oxidation, but both electrochemical reduction and indirect oxidation by the electrogenerated peroxide/hydroxyl radical species at the cathode. The sp^2 hybridized edge-site carbon atoms of the stacked graphene sheets in CNFs were

more susceptible to be attacked by radical oxygen species, thus leading to the higher O/C atom ratio at the cathode. FTIR and XPS results suggested the increased carbonyl and hydroxyl groups but decreased carboxyl groups at the elevated oxidation potential, which was ascribed to the decomposition of carboxyl groups to form carbonyl as well as the formation of more hydroxyl groups at high oxidative potentials. In addition, the O/C atom ratio remained constant with respect to the varied electrode potentials. The reason was that the oxidization occurs only on the external surface of CNFs due to the relatively high crystallinity, and therefore the oxidation degree was independent on the applied potential. These results suggest that the oxidation degree is closely related to the nature of carbon, and the surface with more reactive defect sites tends to achieve a higher electrochemical oxidation degree. Therefore, both electrochemical parameters and material structures are crucial to engineering OFGs by the electrochemical oxidation method.[84-85]

10.1002/chem.202304065

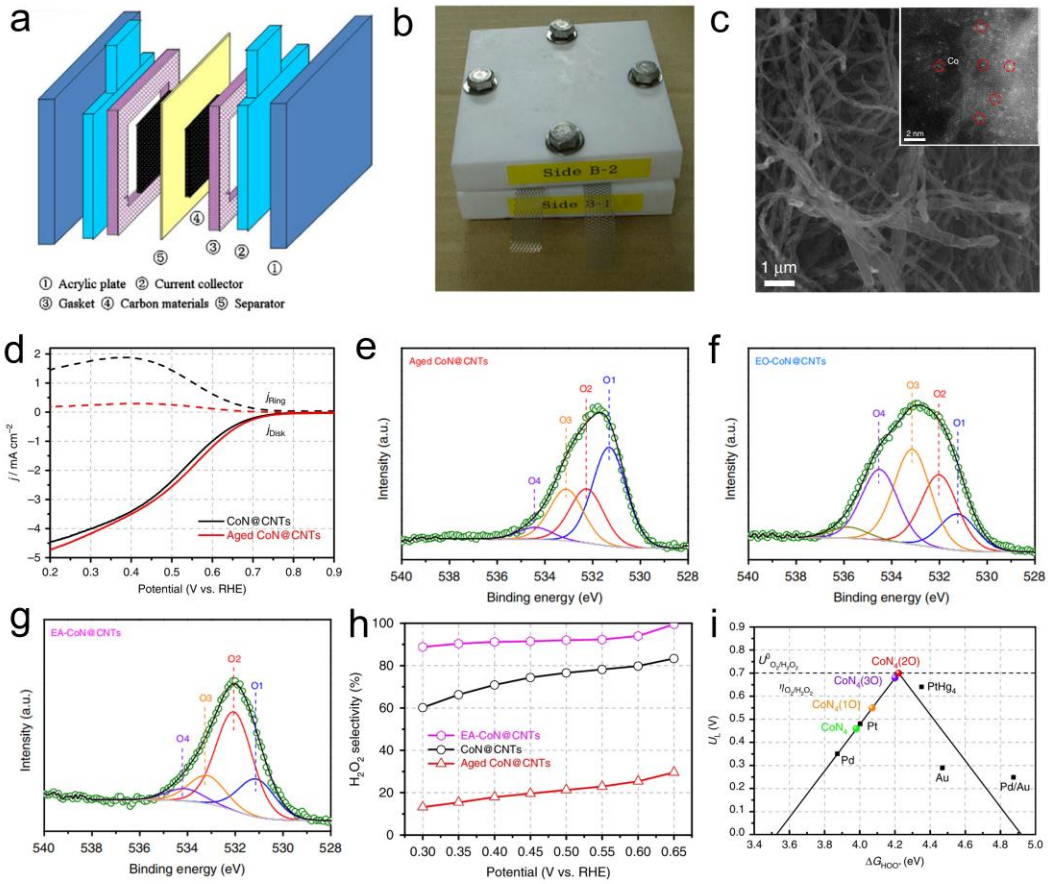

Figure 5. (a) Illustration of the CNF electrode. (b) Photo of the electrochemical cell. Reproduced with permission.[83] Copyright © 2010, Elsevier. (c) SEM images of CoN@CNTs. Inset is the high-resolution TEM image, showing the Co single atom. (d) RRDE measurements of the samples, showing the decreased selectivity to the $2e^-$ ORR after aging. (e-g) XPS O 1s spectra of e) aged CoN@CNTs, f) EO-CoN@CNTs, and g) EA-CoN@CNTs. (h) Selectivity toward the H_2O_2 production of the samples. (i) Calculated volcano plot for the bare CoN_4 moiety and CoN_4 moieties with different epoxy oxygen coverages. Reproduced with permission.[31] Copyright © 2020, The Authors.

In another study,[31] electrochemical treatments were used to reconstruct surface OFGs in aged samples. In detail, OFGs were first modulated near the atomically dispersed Co sites in Co and N co-doped CNTs (CoN@CNTs), as shown in Figure 5c. The obtained CoN@CNTs exhibit obvious ORR current (Figure 5d), and the selectivity toward $2e^-$ ORR is up to 80% in the potential range from 0.5 to 0.7 V. After being exposed to air for ~30 days, however, the selectivity of the aged

CoN@CNTs toward the H_2O_2 production falls dramatically to below 35% over the whole potential range. Electrochemical treatments were then employed to reconstruct OFGs in the aged electrocatalysts. XPS investigations proved that oxygen was the only element that showed noticeable changes during the treatments. In Figure 5e, the O 1s XPS spectra of the aged CoN@CNTs consist of four oxygen species including ketonic oxygen (O1), the oxygen atoms in epoxide or hydroxyl groups and carbonyl oxygen in ester groups (O2), the epoxy oxygen in ester groups (O3), and carboxyl groups (O4). Only the ketonic groups exhibited significant increase from 0.84 at% in the fresh sample to 2.64 at% in the aged sample, indicating the crucial role of ketonic groups on the $2e^-$ ORR selectivity. The aged CoN@CNTs underwent a two-step electrochemical activation (EA) including an electrochemical oxidation (EO) and an electrochemical reduction (ER) to reconstruct surface OFGs.[31] After the EO process, more ester groups (O2) and carboxyl groups (O4) are produced (Figure 5f), while ketonic oxygen (O1) is decreased. EA-CoN@CNTs are then obtained after a subsequent ER treatment that results in the reduction of ester and carboxyl groups under the cathodic potential, while epoxy groups are thermodynamically more stable and are hard to be removed by the electrochemical reduction treatment (Figure 5g). The EA-CoN@CNTs exhibit a high $2e^-$ ORR selectivity up to 90% within the potential region between 0.3 and 0.6 V, superior to the freshly-prepared samples (Figure 5h). DFT calculations revealed epoxy groups depleted the electrons around Co atoms in CoN_4 moieties, and hence optimized the ΔG_{OOH*} at the nearby Co-N_4 sites (Figure 5i). The dissociation energy of OOH* at

Co-N_4 site was also increased, which facilitated the preservation of O–O bonds in OOH* intermediates and thus the enhancement of the $2e^-$ ORR selectivity. This work not only provides a feasible way to modulating the OFGs in oxygen-rich carbon materials by electrochemical treatments, but also systematically discusses the contribution of epoxy groups to the $2e^-$ ORR with the presence of Co metal sites.

2.3 Precursor inheritance

In addition to chemical and electrochemical oxidation methods, OFGs can also be inherited from oxygen-containing precursors. Graphene oxide (GO) is a typical carbon material with high oxygen content, but the excess oxygen atoms in GO disrupt the electron distribution around carbon and decrease the electronic conductivity, severely. Therefore, it is easy to obtain OFG-enriched graphenes by removing excessive OFGs in GO. For example, it was demonstrated that a strong alkaline environment can effectively remove OFGs from GO surface.[61] Therefore, rGO-KOH was prepared by a hydrothermal treatment of GO in a KOH solution at 80 °C, and meanwhile, rGO-KBH_4 was also prepared via a chemical reduction by stirring GO in a KBH_4 solution.[56] The surface of the obtained rGO-KBH_4 was dominated by hydroxyl groups, while the rGO-KOH possess abundant ether groups that were highly active toward the $2e^-$ ORR.[56] Compared with rGO-KBH_4, rGO-KOH exhibited higher selectivity and activity owing to a higher percentage of ether groups and a larger electrochemically active surface area. In this work, OFGs are inherited from GO precursors via two different methods, demonstrating the effectiveness of such precursor inheritance strategy.

10.1002/chem.202304065

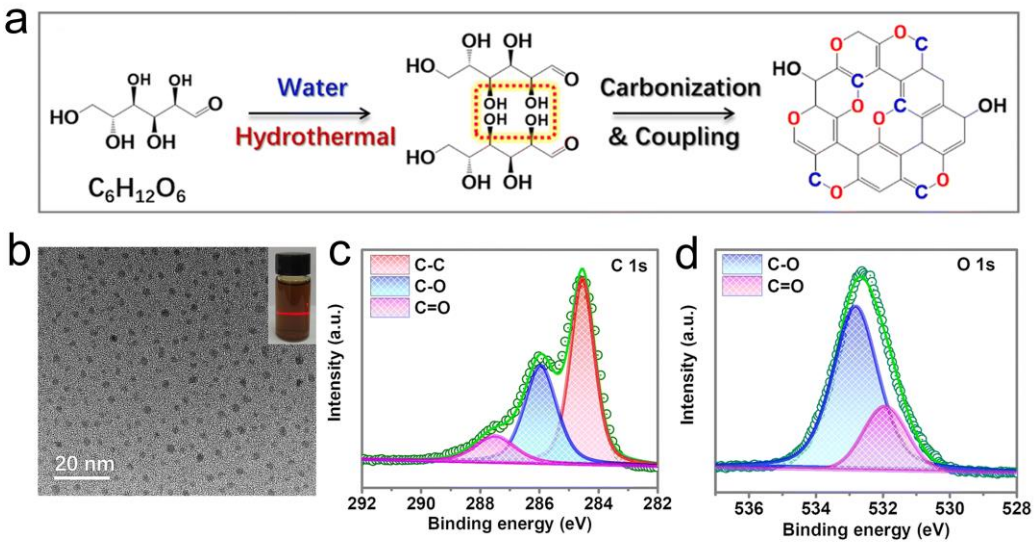

Figure 6. (a) Illustration of the preparation scheme for oxygen-rich CQDs. (b) The TEM image of the COQs. The inset is the photograph of the CQDs dispersing in water, exhibiting the Tyndall effect. (c) C1s and (d) O 1s XPS spectra of CQDs. Reproduced with permission.[54] Copyright © 2022, The Royal Society of Chemistry.

Moreover, oxygen-rich carbon materials can also be obtained by the carbonization of oxygen-containing precursors such as polymers,[86-87] biomass,[88] and coals,[89-91] where OFGs in the precursors may be preserved during the carbonization process. For example, Guo et al. prepared carbon quantum dots (CDQs) with a high oxygen content using glucose as the carbon source.[54] As depicted in **Figure 6**a, glucose molecules first undergo dehydration to form aromatic compounds and oligosaccharides, and then dehydrated glucose molecules are carbonized and combined together by the crosslinking of the resultant CQDs and C–O–C bonds. Transmission electron microscopy (TEM) image shows the homogeneous dispersion of the sample with a narrow size distribution (Figure 6b). The initial carbonization and nucleation processes of glucose molecules and the growth of the nuclei are determined by the temperature, treatment time, and precursor

concentration; therefore, the size of CQDs can be tuned by regulating these parameters. The oxygen content in CQDs can reach up to 30.4 at%. High-resolution C1s and O1s XPS spectra in Figure 6c-d suggest the existence of both C–O containing and C=O containing OFGs, with an apparently higher ratio of the C–O related OFGs. As a result, the O-rich CQDs catalyst showed nearly 100% selectivity toward the $2e^-$ ORR. Experimental and theoretical investigations indicated that the carbon atoms in C–O of etheric groups are the most active sites. This work demonstrated the precursor inheritance strategy was also an effective strategy to synthesize carbon materials with high oxygen content.

2.4 Other methods

Oxygen plasma treatment have also been used to construct OFGs on carbon surface,[6, 60, 92] and the formation mechanism is similar to chemical oxidation. Wang et al. introduced abundant OFGs into CB successfully using a one-step oxygen plasma treatment (**Figure 7**a),[6] but a large number of defects were also introduced in the obtained sample (CB-Plasma). Therefore, to explore the relation between OFGs and defects, oxygen plasma was replaced by UV-ozone atmosphere, and the obtained CB-UV possessed abundant OFGs but few defects. Also, OFGs in CB-Plasma were further removed by annealing in Ar atmosphere (CB-A) for comparison. Based on the XPS results (Figure 7b), the oxygen content was increased from 0.8% (CB) to 8.5% and 23.5% for CB-UV and CB-Plasma, respectively. Moreover, the O1s XPS spectra demonstrated the similar ratio of C–O containing to C=O containing OFGs for CB-UV and CB-Plasma. In Figure 7c, CB-Plasma

showed a high onset potential (0.1 mA cm^{-2} at 0.8V) and nearly 100% selectivity at 0.6 V, superior to those of CB-UV. Interestingly, the OFG-free CB-A exhibited similar electrochemical performance to the OFG-enriched CB-Plasma, indicating that the performance originates from the defective carbon structure instead of OFGs. DFT calculations were performed to explore the role of OFGs here (Figure 7d-e). The results revealed that the presence of oxygen atoms promoted the adsorption of OOH* at defective sites. As for the defect-free pristine graphene nanoribbon (GNR), however, the decoration of oxygen weakened the OOH* adsorption drastically, resulting in the shift of ΔG_{OOH*} from one side to the other side of the volcano plot. Consequently, the CB-Plasma exhibited higher activity than CB-UV owing to the synergy between OFGs and defects. This work suggests nonnegligible roles of defects in carbon materials, which contradicts most of other studies where bare defects are believed to be catalytically inactive.[19, 93] The inconsistency between various studies might be ascribed to the different structures of carbon materials due to the varied preparation procedures.

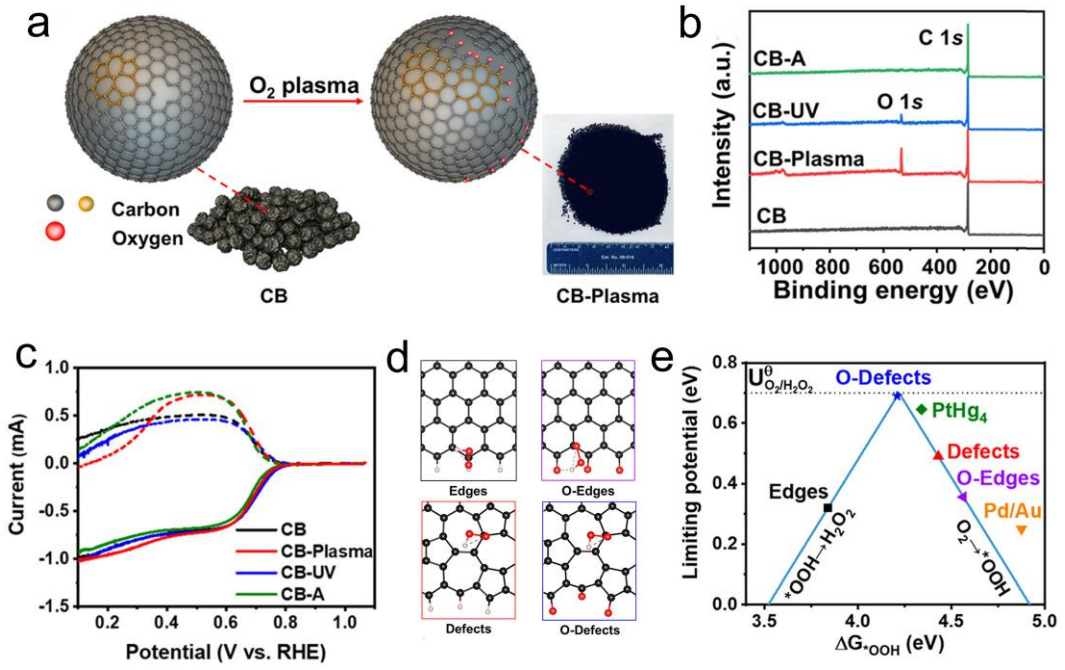

Figure 7. (a) Illustration of the preparation of CB-Plasma. (b) XPS survey spectra of CB, CB-Plasma, CB-UV, and CB-A. (c) Polarization curves of the samples on RRDE at 1600 rpm in O_2-saturated 0.1 M KOH (solid line: disk current; dashed line: ring current). (d) Optimized OOH* structures adsorbed on the active sites. Color code: C, black; O, red; and H, white. (e) The calculated volcano relation of the limiting potential U_L as a function of ΔG_{OOH*}. Reproduced with permission.[6] Copyright © 2021, American Chemical Society.

In another work, Chu et al. employed a straightforward method to construct OFG-modified CNTs, specific aromatic organic molecules were used as model precursors for different OFGs and were attached on CNTs through π–π interactions using a solvothermal method.[94] In specific, 9-phenanthrenol (PE), 9-phenanthrenecarboxylic acid (PCA), phenanthrenequinone (PQ), and xanthene (X) were selected as the model precursors for hydroxyl, carboxyl, carbonyl, and epoxide groups, respectively. The results indicated that carbonyl groups possessed the highest activity, followed by the carboxyl groups, toward the $2e^-$ ORR, while the differences between the zigzag or armchair configurations of carbonyl groups were

negligible. It should be noticed that the structures of aromatic organic molecules were preserved during the solvothermal treatment. Therefore, although strong interactions between the model molecules and CNTs were demonstrated by XANES and XPS results, it is still questionable whether OFGs play the same role here as compared with OFGs anchoring on CNT surface directly.

3 Roles of OFGs in the 2e⁻ ORR

In general, carbon-based materials such as graphite, graphene, and CNTs are inert in catalysis owing to their sp^2-hybridized carbon matrix,[95] and the surface of carbon is usually hydrophobic due to the weak interaction with H_2O molecules.[96] Introducing OFGs can improve the hydrophilicity of carbon since hydrogen bonds may form between OFGs and H_2O molecules. This will change the adsorption behavior of O_2 and H_2O molecules on carbon sites, and hence influence the catalytic performance toward the 2e⁻ ORR. Moreover, OFGs can efficiently modulate the local electronic structures of the carbon matrix, and this is perhaps the most important role of OFGs in oxygen-rich carbon electrocatalysts.[97-103] Also, defects and metal species such as single atoms, nanoparticles, or metal oxides should not be neglected with regard to tuning local electronic structures of carbon. In the following sections, we first review the contribution of different OFGs to the 2e⁻ ORR and then discuss the interplay between OFGs and metal species or defects.

3.1 Intrinsic activity of different OFGs

Considering the nature of catalysts, one of the most concerned problems is that which specific OFG possess the most significant contribution to accelerating the 2e⁻

ORR. A variety of studies tried to correlate the electrocatalytic performance of carbon-based catalysts with the varied OFGs, aiming to disclose the most active species. For example, Wang et al. tuned the ratio of OFGs in CB including aldehyde, epoxide, and carbonyl by annealing CB in air at 500 °C for different time (5, 15, 30, 45, and 60 minutes).[51] Their experimental results and theoretical investigations demonstrated that epoxide and aldehyde groups contribute more to the H_2O_2 production. In another work,[57] carbonyl groups were reported to promote O_2 adsorption by creating nucleophilic sites at adjacent carbon atoms, while epoxide groups may possess the best activity but were less favorable for O_2 adsorption. In general, both C=O containing OFGs and C–O containing OFGs have been reported as the most active species toward the $2e^-$ ORR, which may be ascribed to the varied carbon matrix structure and the different exploration methods.

A major challenge for evaluating the specific role of different OFGs is that there is usually more than one type of OFGs in carbon. As described in Lu et al.'s work,[19] the O-CNTs exhibited high activity and selectivity toward the $2e^-$ ORR, but there were both C–O containing and C=O containing OFGs. Therefore, to exclude the possible synergistic effect between different OFGs, the pristine CNTs were deliberately engineered with C=O containing OFGs by a hydrothermal treatment in KOH solution or C–O containing OFGs by co-pyrolysis with polyethylene oxide (PEO). The obtained CNTs-PEO exhibited higher activity, indicating the more critical role of epoxide groups. Further, ΔG_{OOH*} values were calculated using a two-dimensional graphene with different OFGs at varied locations as the model (**Figure**

8a), and the results are displayed in the volcano plot in Figure 8b. The calculated U_L for the $2e^-$ ORR are only 0.02 and 0.06 V for epoxide groups on the basal plane (O basal 1) and the edge of graphene (O edge), respectively. Among different –COOM functional group (M=H or Na) configurations, the armchair carboxyl edge (–COOM edge 2) is the most active one. As for hydroxyl groups, the calculation demonstrated low intrinsic activity. This work provided fundamental understandings on the contribution of different OFGs in the $2e^-$ ORR.

Later, Wu et al. provided experimental insights into the different intrinsic activity of carboxyl groups and hydroxyl groups.[93] The authors discovered that cationic surfactants, cetyltrimethylammonium bromide (CTAB) for example, can promote the $2e^-$ ORR on CB by providing a Coulombic pull to weaken the adsorption of peroxide intermediates, resulting a high selectivity up to 95.2% in alkaline media.[93] Therefore, CB powders were further engineered with additional OFGs by liquid chemical oxidation with concentrated HNO_3. Under the Coulombic pull, carboxyl groups possessed weak OOH* binding energy and hence promoted the desorption of the as-formed H_2O_2. Although carbonyl groups also participated in the $2e^-$ ORR, they exhibited strong OOH* binding energy that resulted in the reduction of H_2O_2 in low potential region. In contrast, hydroxyl groups contributed little to the $2e^-$ ORR as they cannot create electron-rich nucleophilic sites for O_2 adsorption. These works demonstrated the positive roles of carboxyl and carbonyl groups in facilitating the adsorption of O_2 molecules and reaction intermediates, while hydroxyl groups were typically believed to possess little effect.

10.1002/chem.202304065

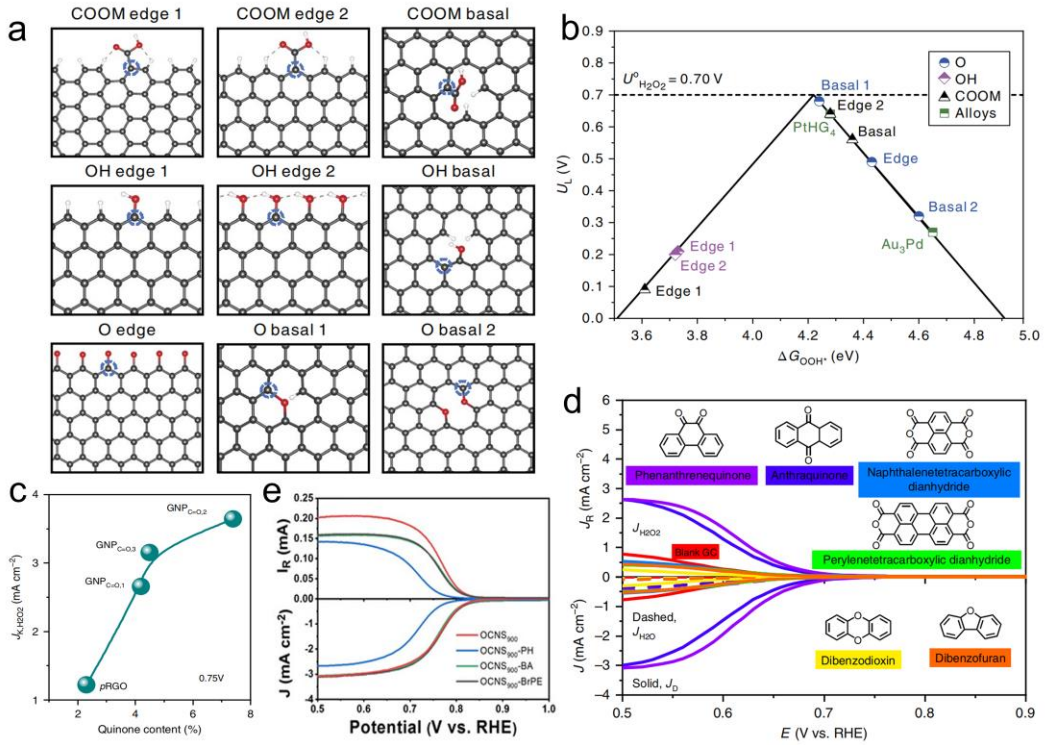

Figure 8. (a) The structure models of different OFG configurations for the DFT calculation. The carbon atoms denoted by a blue circle are the active sites under investigation (M = H and Na). (b) The calculated 2e⁻ ORR-related volcano plot. Reproduced with permission.[19] Copyright © 2018, Springer Nature. (c) The $J_{K,H2O2}$ of the catalysts as a function of quinone content. (d) The electrocatalytic performance of standalone molecules toward 2e⁻ ORR. Reproduced with permission.[28] Copyright © 2020, The authors. (e) ORR polarization curves of the samples on RRDE. Reproduced with permission.[30] Copyright © 2021, John Wiley and Sons.

In another work, carbon-based electrocatalysts were deliberately engineered with specific OFGs to reveal the most active OFG.[28] As mentioned earlier, different types of OFGs were introduced into GNPs using a two-step gas-phase chemical oxidation method.[28] The onset potentials indicated that the samples with carbonyl-related groups including quinone and carboxylic acid groups were more active as compared with those with in-plane etheric rings. Next, the contents of quinone and carboxylic acid groups in the catalyst were tuned by a chemical leaching method. Interestingly, the calculated kinetic current $J_{K,H2O2}$ shows a linear positive

correlation with the content of quinone groups, as displayed in Figure 8c. Furthermore, the authors investigated the performance of standalone molecules with specific OFGs including phenanthrenequinone, anthraquinone, naphthalenetetracarboxylic dianhydride, perylenetetracarboxylic dianhydride, dibenzodioxin, and dibenzofuran. The results proved that only those possessed quinone groups, i.e. phenanthrenequinone and anthraquinone, were active toward the $2e^-$ ORR (Figure 8d). Although these OFG-containing standalone molecules are not the same as the oxygen-rich carbon electrocatalysts in nature, the results do provide relevant insights into the role of OFGs in the $2e^-$ ORR for reference. DFT calculations were performed to explore the difference between quinone groups at the varied locations. It was then suggested that quinone groups at both the edge and the basal were active, and they were prone to form at the edge site owing to the relatively lower energy for breaking the sp^2 C–C bonds.

The different contribution of specific OFGs can also be distinguished by the selectively blocking strategy.[30] Chen et al. prepared oxygen-doped carbon nanosheet ($OCNS_{900}$) electrocatalysts for the $2e^-$ ORR. During the chemical reaction, the carbonyl, hydroxyl, and carboxyl groups in the $OCNS_{900}$ catalysts were selectively blocked by phenylhydrazine (PH), benzoic anhydride (BA), and 2-bromo-1-acetophenone (BrPE), respectively, and therefore the contribution of each type of OFGs could be evaluated by the decreased catalytic activity. Figure 8e shows the polarization curves of the bare $OCNS_{900}$ before and after the selective blocking. All the catalysts exhibited somewhat decreased performance after the blocking,

indicating the general contribution of the OFGs to the 2e⁻ ORR. Moreover, the most significant activity decrease was observed after blocking carbonyl groups, suggesting the higher contribution of carboxyl groups on the 2e⁻ ORR than hydroxyl and carboxyl groups. In another work,[104] the roles of OFGs were evaluated using a similar blocking strategy; however, the results demonstrated higher activity of carboxyl groups at the edge sites than carbonyl groups.[104] Clearly, the selective blocking strategy serves as an effective approach to explore the role of OFGs. However, the adsorption of special molecules at OFG sites may also exert significant impact on the nature of active sites, which should be taken into consideration in future studies.

3.2 Interplay of OFGs and metal species

Metal species such as single atoms, nanoparticles, or metal oxides are commonly introduced into carbon-based electrocatalysts and serve as active sites. For instance, carbon-supported single atom catalysts (SACs) have drawn considerable attention in many reactions,[105-108] and in particular, a large number of M–N_4 species have been demonstrated as active sites for the 4e⁻ ORR.[109-110] Besides, it was revealed by DFT calculations that highly oxophilic Ru, Fe, and Co sites facilitate the breaking of O–O bond in OOH* and hence are selective for the 4e⁻ ORR, while Ni, Ag, and Pt sites with lower oxophilicity are more prone to the protonation of OOH* to produce H_2O_2.[21] In these metal-containing carbon-based catalysts, OFGs can effectively modulate the electronic structure of metal species, and meanwhile, OFGs and metal species may tune the electronic structure of carbon, synergistically.

The adsorption of electron-rich O* near Co–N_4 moieties will increase the charge state of the Co center of Co–N_4 and hence increase the ΔG_{OOH*}, as reported in Hyeon's work.[21] **Figure 9**a shows the ΔG_{OOH*} of Co–N_4 moieties with various adsorbates, and Figure 9b illustrates the corresponding electron distribution structures. The ΔG_{OOH*} was increased from 3.9 eV to 4.1 and 4.5 eV after the adsorption of one and two O* near the Co–N_4 moiety, respectively.[21] The adsorption of the electron-rich OH* results in the similar trend, while the adsorption of electron-deficient H^+ leads to the opposite. Further, Co_1–NG(O) SACs with highly oxidized Co centers were prepared where Co–N_4 moieties were modified by epoxide groups, and Co_1–NG(R) composed of electron-rich Co centers were also prepared for comparison. Not surprisingly, the Co_1–NG(O) SACs exhibited high selectivity toward the $2e^-$ ORR (~ 80%) in 0.1 M KOH, superior to either Co_1–NG(R) or NG(O) without Co centers (Figure 9c), highlighting the interactions between OFGs and Co–N_4 moieties.

10.1002/chem.202304065

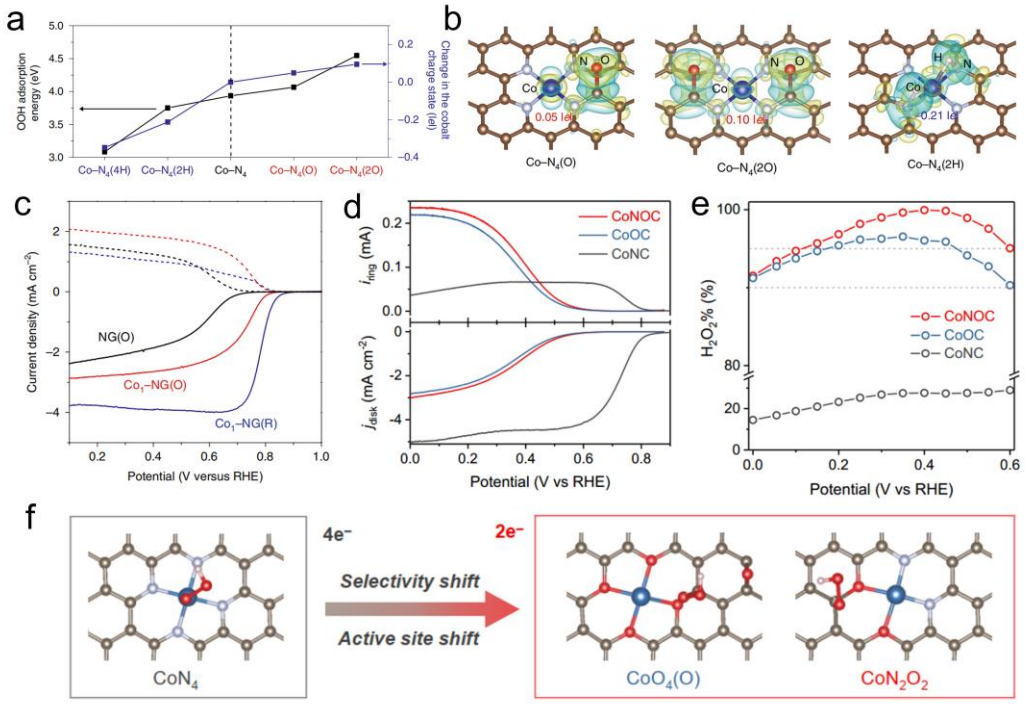

Figure 9. (a) Calculated OOH* adsorption energies and relative charge states of the cobalt metal site. (b) Differential charge densities of Co–N_4/graphene after the adsorption of O*, 2H*, or 2O* near the cobalt atom. Yellow and cyan isosurfaces (±0.003 $Bohr^{-3}$) show the electron gain and electron loss, respectively. (c) LSV of ORR at 1,600 rpm (solid lines) and the H_2O_2 detection current densities at the ring electrode (dashed lines) for different catalysts in 0.1 M KOH. Reproduced with permission.[21] Copyright © 2020, Springer Nature. (d) LSV curves of ORR in O_2-saturated 0.10 M $HClO_4$, showing the disk current density (j_{disk}) and ring current (i_{ring}). (e) Calculated H_2O_2 selectivity at different applied potentials. (f) Geometry structures of OOH* adsorption on different moieties, showing the change of active center. Reproduced with permission.[50] Copyright © 2021, American Chemical Society.

Similarly, it was demonstrated that the ORR selectivity of Co-SACs could be tuned by modulating the first and second coordination spheres of Co centers; in other words, it was the molecular-level local structure of Co centers that determined the overall reaction pathway.[50] A series of Co-SACs with varied coordination environment including CoNC, CoNOC, and CoOC were prepared, and the polarization curves and the calculated selectivity toward the ORR are displayed in

Figure 9d-e. The CoNC SACs exhibit a high onset potential of ~0.84 V and a low selectivity (< 30%) toward the $2e^-$ ORR, while CoNOC and CoOC show a low onset potential of ~0.57 V and a high $2e^-$ ORR selectivity (>95%) over a wide potential range. Based on DFT calculations, increasing the oxygen atoms in the first coordination sphere around Co lowered the electronic density of Co and decreased the corresponding ΔG_{OOH*}. The ORR selectivity is altered from the $4e^-$ ORR path to the $2e^-$ path accompanied by the shift of active sites from the Co atoms to the O-adjacent C atoms (Figure 9f). In addition, this work also discussed the role of Co. Specifically, the metal-free moieties possess high selectivity toward $2e^-$ ORR but deficient activity, and incorporating Co single atom can provide additional electrons to the structure, thereby boosting the reaction.[50] However, it has also been reported in another work that the direct contribution of Co single atom and Co metal toward the $2e^-$ ORR was negligible, and the presence of Co played a significant role in the graphitization process of carbon, and the formation of defects and OFGs.[111]

While Co-N_4 and Fe-N_4 are typically reported as active species for the $4e^-$ ORR,[112-113] Jiang et al. discovered the critical role of oxygen atom in modulating the ΔG_{OOH*} of metal-containing carbon, and Fe-O-C moieties were proposed as active sites toward the $2e^-$ ORR.[114] A series of transition metal (Fe, Pd, Co, and Mn) single atoms are anchored into CNT vacancies (Fe-CNT, Pd-CNT, Co-CNT, and Mn-CNT), and the neighboring C, O, or N coordination was tuned for the $4e^-$ or $2e^-$ ORR pathway. **Figure 10**a shows the TEM image of Fe-CNTs. The LSV curves of the Fe-CNT samples are displayed in Figure 10b, where the Fe-CNT shows high selectivity

toward the 2e⁻ ORR, and the selectivity is decreased after a reduction treatment of Fe-CNT in forming gas (red. Fe-CNT). When nitrogen-doped CNT was used as the support, the O atom was replaced with N, and the electron transfer number was increased from 2.09 for Fe-CNT to 3.71 for Fe-N-CNT as the formation of Fe–C–N coordination. DFT calculations provide theoretical insights into the active sites. As illustrated in Figure 10c, without oxygen, most Fe and C atoms are located at the left leg of the volcano plot, which bind OOH* too strongly that promote the dissociation of the O–O bond. Once oxygen atoms are incorporated, most C atoms in the vicinity of Fe-C-O motifs are located at the right leg of the volcano plot, and thus facilitating the 2e⁻ ORR. Meanwhile, compared with those C atoms with only O dopants, the presence of Fe atoms can further strengthen the OOH* binding on C sites; that is, Fe and O atoms modulate the electronic structure of C atoms in Fe-O-C moieties, collectively. This work highlights the contribution of oxygen in tuning the local electronic structures of carbon, which has been generally overlooked. In another work, DFT calculation demonstrated that the ΔG_{OOH*} on carbon can be regulated synergistically by the embedded Co nanoparticles (NP) and surface OFGs.[49] Following the theory guidance, the authors further prepared Co NPs-encapsulated porous carbon nanocages with abundant C–O–C surface groups, and the optimized catalyst showed a high selectivity of 94% toward the 2e⁻ ORR in 0.1 M $HClO_4$.

10.1002/chem.202304065

WILEY-VCH

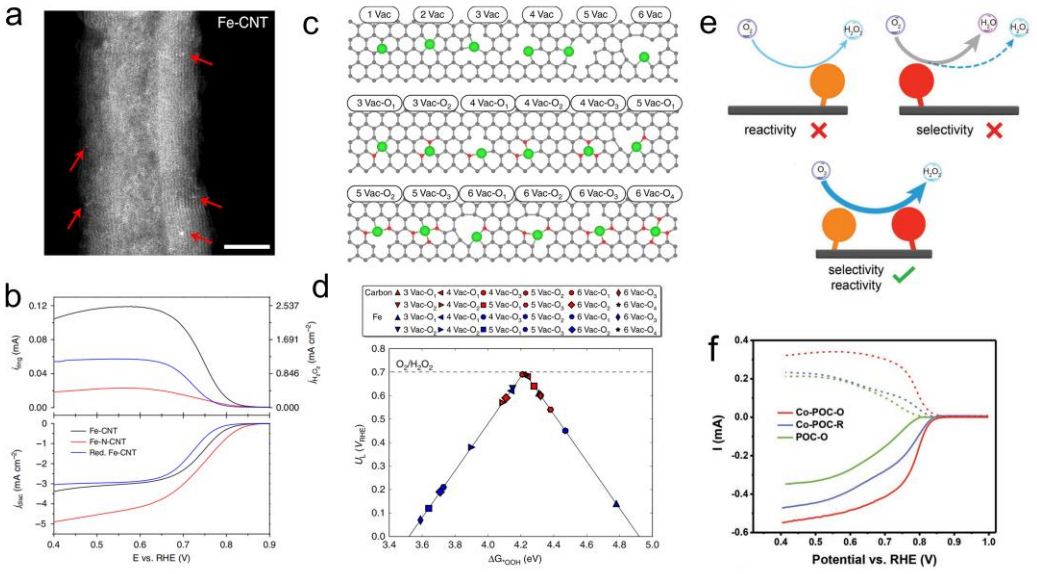

Figure 10. (a) TEM image of Fe-CNT. (b) LSV curves and H_2O_2 detection current of Fe-CNT, Fe-N-CNT, and Red. Fe-CNT. (c) Structure models of the examined configurations for single Fe atom coordinated in two-dimensional carbon material with and without O species. Green, red, and gray colors denote Fe, O (or N), and C atoms, respectively. (d) The calculated ORR activity volcano plot for the $2e^-$ pathway to H_2O_2. Red and blue symbols indicate OOH* adsorption at C and Fe, respectively. Reproduced with permission.[114] Copyright © 2019, The Authors. (e) Schematic of the synergistic strategy of atomic Co−N*x*−C sites and OFGs for H_2O_2 electrosynthesis. (f) LSV curves of the samples. Reproduced with permission.[115] Copyright © 2019, John Wiley and Sons.

Recently, Li et al. demonstrated complementary contributions of OFGs and metal species (Co-N*x*-C) toward the ORR. As illustrated in Figure 10e, OFGs facilitate the high selectivity but possess sluggish kinetics, while Co–N*x*–C sites contribute to fast ORR kinetics but suffer from low selectivity.[115] The Co-POC-O sample containing both atomic Co–N*x*–C sites and OFGs was prepared by pyrolyzing cobalt-coordinated porphyrin framework (Co-POF), followed by chemical leaching and chemical oxidation with HNO_3 solution for removing Co NPs and constructing OFGs, simultaneously. Co–POC–R without OFGs, and POC–O without Co–N*x*–C sites were obtained via similar procedures. Figure 10f displays the polarization

curves of the samples, and the Co-POC-O with both Co–N*x*–C sites and OFGs exhibited the best performance, suggesting the synergistic effect between Co sites and OFGs toward the efficient H_2O_2 production.

To sum up, numerous studies have suggested that both OFGs and metals species are effective in modulating local electronic structures that exert significant effects on the catalytic performance of carbon materials. More specifically, metal species without OFGs such as M-N_4 species are generally more selectivity toward the $4e^-$ ORR. In other cases where metal species are strongly coupled with OFGs, the metal-based species, Fe-O-C moieties for example, can serve as active sites for the $2e^-$ ORR owing to the synergistic effect between metal species and OFGs.

3.3 Interplay of OFGs and defects

During the construction of OFGs, structure defects may be inevitably introduced,[116-117] and the defect sites were also believed to contribute to the $2e^-$ ORR of carbon-based electrocatalysts.[118] Although bare defective carbon sites have been demonstrated as active sites of the CB-Plasma toward the $2e^-$ ORR,[6] more studies suggested that bare defect sites without oxygen are inactive.[19, 93] For example, to identify the role of surface defects, Wu et al. prepared two different samples with saturated sp^3 edge (sd rCB) or unsaturated sp^2 edge (ud rCB) by calcinating the oxidized carbon black (OCB-120) at 800 ℃ under the atmosphere of reduction (H_2) or inert (Ar) for 2h, respectively.[93] The OFGs at the outer-most surface were removed by the thermal treatment, and the activity and selectivity were

decreased, accordingly. This work indicates that bare defects were not active toward the 2e⁻ ORR without OFGs.

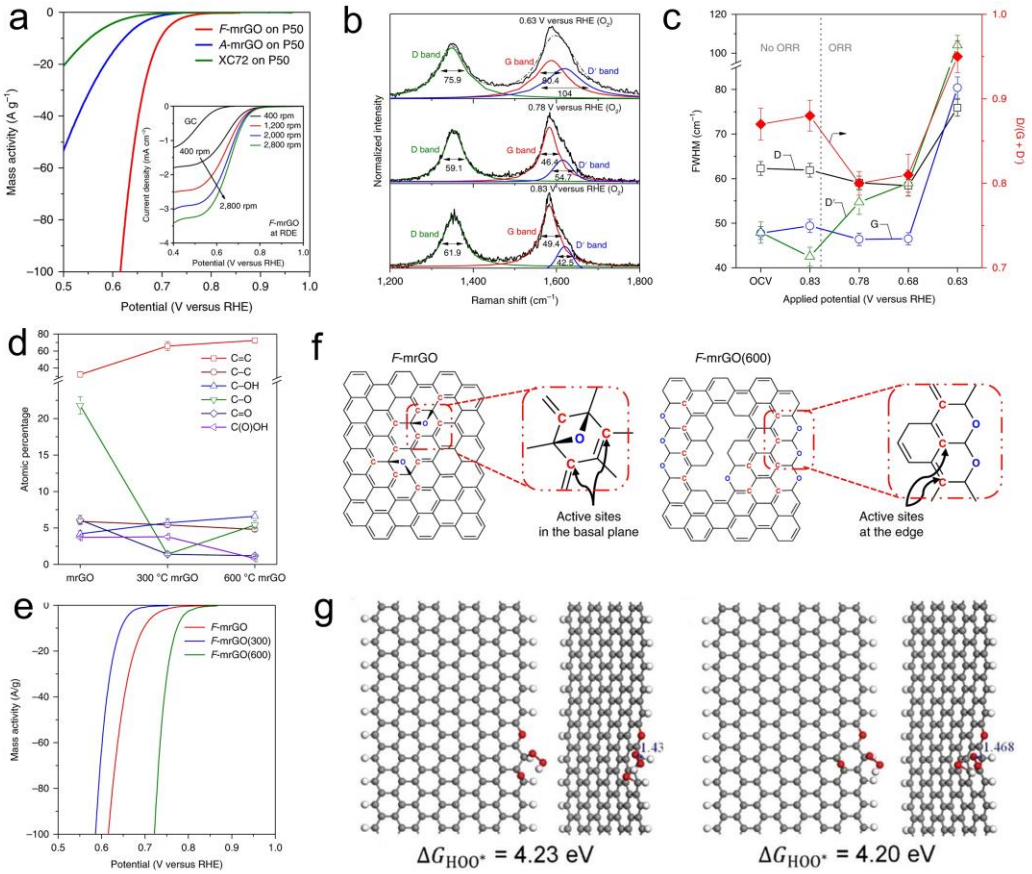

Figure 11. (a) LSV curves of *F*-mrGO, *A*-mrGO and XC72-based electrodes loading on P50 porous carbon paper as the support in O_2 saturated 0.1 M KOH. (b) *In situ* Raman spectra—with calculated Voigt deconvolutions—of *F*-mrGO at various potentials. (c) FWHM and D/(G + D′) ratio of *F*-mrGO electrodes as a function of applied potentials. (d) atomic ratio of the as-prepared, unannealed mrGO, and annealed mrGO powders (300 and 600 °C) measured by C1s XPS. (e) LSV curves of the as-prepared and the annealed *F*-mrGO in O_2 saturated 0.1 M KOH. (f) Illustration of the proposed low-overpotential active sites on *F*-mrGO and *F*-mrGO(600). Reproduced with permission.[20] Copyright © 2018. Springer Nature. (g) The optimized structure configurations of the two most active 1ET + 1EP structures after the adsorption of HOO* at the active site. The grey, red and white balls represent the C, O and H atoms, respectively. Reproduced with permission.[119] Copyright © 2019. The Royal Society of Chemistry.

Recently, Kim et al. reported that the 2e⁻ ORR is related to edge-site defects, and sp^2-hybridized carbon near-ring ether defects along sheet edges are most active.[20]

Mildly reduced graphene oxide (mrGO) was prepared by dispersing GO in water and stirring under nitrogen flow at 100 °C, and few-layered mrGO (*F*-mrGO) electrodes were prepared by immersing a piece of P50 carbon paper in a 0.05 wt.% mrGO solution for 1 min followed by immediate drying. In contrast, mrGO aggregation (*A*-mrGO) on P50 carbon paper was obtained using a more conventional drop-casting method, in which the well-dispersed mrGO solution was dropped onto P50 substrate and dried. The LSV curves were recorded in O_2 saturated 0.1 M KOH solution (**Figure 11**a), and the *F*-mrGO exhibits superior electrochemical activity to *A*-mrGO and activated carbon (XC72). The *in situ* Raman spectra are shown in Figure 11b, and the FWHM and the D/(G + D′) ratio at different potentials are displayed in Figure 11c. The D′ band was increased and broadened, while D and G band remained constant in low overpotential region, indicating that certain sp^2-hybridized carbon sites in basal plane were active. When the applied potential was decreased to 0.63 V, D′ and G band were also broadened, suggesting that the edge sites, and/or sp^3-hybridized carbon defects were also interacted with adsorbates. *F*-mrGO electrodes were further annealed at 300 °C or 600 °C under N_2 atmosphere, and the obtained samples were denoted as *F*-mrGO(300) and *F*-mrGO(600), respectively. The presence of various OFGs including ether, hydroxyl, ketone and carboxylic acid groups is demonstrated by the XPS results (Figure 11d).[20] The amount of C–O and C=O species were decreased but sp^2 carbon was increased after annealing at 300 °C, indicating that the thermal treatment substantially reduced OFG-associated carbon defects. After annealing at

600 °C, the catalyst showed a dramatic decrease in carboxyl group and a modest increase in ether group, in consistent with the thermal decomposition of carboxyl to generate additional ether groups.[72] Unexpectedly, *F*-mrGO(600) is more active than *F*-mrGO considering its low oxygen content. The authors further explored the active sites by combining additional characterization results including XPS, FTIR, and NEXAFS, and the proposed active sites are illustrated in Figure 11f.[20] In short, epoxy or ether ring groups located on either basal planes or plane edges were all critical to oxygen-rich carbon catalysts for achieving high activity in alkaline media. Soon later, Kim et al. also demonstrated the similar principle in nitrogen-doped rGO (N-rGO) that certain carbon defects associated with epoxy or ether groups possess crucial influence on facilitating the $2e^-$ ORR.[120] However, Tan et al. discussed the $2e^-$ ORR activity of different OFGs structures on mrGO using DFT calculation systematically, and they reported that the activity of the proposed active sites in the *F*-mrGO were very low.[119] Instead, two different OFGs structures were proposed with even higher activity than the state-of-the-art $PtHg_4$ electrocatalyst, namely 2EP consisting two neighboring ether (EP) groups located close to the mrGO sheet edges, and 1ET+1EP consisting a ring ether (ET) group and an EP group along the mrGO sheet edge (Figure 11g). Moreover, the graphene edge sites and the synergetic effects between different OFGs were also essential for the high $2e^-$ ORR activity of mrGO. Similar to the interplay between OFGs and metal species, the defects in carbon usually modulate local electronic structures collectively with OFGs. Although it has been reported that some specific defect sites such as edge-site

defects can serve as active sites, more studies have demonstrated that bare defects are not active toward $2e^-$ ORR unless they are associated with certain OFGs.[19, 93]

4 Conclusions and perspectives

To sum up, OFGs have been demonstrated as the key to rendering oxygen-rich carbon materials with high electrocatalytic performance toward the $2e^-$ ORR. There are basically two major methods to prepare oxygen-rich carbon materials based on the source of oxygen atoms. For one, OFGs can be introduced from the outside to the surface of carbon matrix by chemical/electrochemical oxidation reactions, and common oxidants include HNO_3, $KMnO_4$, H_2O_2, air, O_3, plasma, etc. The original sp^2 C–C bond must be broken to form new C–O or C=O hybridizations; therefore, defects and even structural damages are easily introduced. For the other, oxygen-rich carbon-based electrocatalysts can also be prepared by pyrolyzing oxygen-containing precursors such as glucose and epoxy or by removing excessive OFGs from specific oxygen-rich carbon such as GO. The oxygen content can be increased by extending the oxidation treatment time, increasing the ratio of oxidant, selecting high oxygen-containing precursors, etc. It is worth noting that the increased oxidation temperature does not necessarily result in a higher oxygen content in oxygen-rich carbon electrocatalysts, because the high-temperature treatment would lead to the decomposition of OFGs and hence may decrease the oxygen content. On the other hand, the type of OFGs can be roughly adjusted based on their varied thermal stability, and the COOH groups are commonly regarded as the least stable

OFG that can be easily removed. The distribution of OFGs is closely related to the structure of carbon matrix, and OFGs are prone to form at edge and defect sites owing to the lower formation energy compared with those at the basal site. In short, the content, type, and distribution of OGFs in oxygen-rich carbon electrocatalysts are determined collectively by multiple factors including treatment time, temperature, the nature of carbon and oxidants, etc. These complex factors pose tremendous challenges to the precise modulation of OFGs. Customized methods based on materials structural characteristics and physicochemical properties are required so as to regulate the OFGs in oxygen-rich carbon materials at will. As for the roles of OFGs in oxygen-rich carbon electrocatalysts for the $2e^-$ ORR process, tuning the local electronic structures is perhaps one of the most important functions. The electronic structures of sp^2 hybridized carbon atoms are thermodynamically not favored for the adsorption of O_2 and OOH*. Introducing OFGs such as carbonyl, epoxide, and the carboxyl would create electron-rich nucleophilic active sites owing to the lone pairs of the oxygen atoms, and the higher charge density would increase the ΔG_{OOH*}. Also, OFGs and other species such as metals or carbon defects may tune the electronic structure of carbon synergistically, and hence create new types of active sites, Fe–O–C moieties for example. Although the roles of bare defects are still under debate, most studies insist that defects can contribute to the $2e^-$ ORR only when OFGs are present. Furthermore, OFGs may still accelerate the reaction by creating hydrophilic surface.

Until now, there are a lot of controversies regarding the most active OFGs in

oxygen-rich carbon electrocatalysts. Various OFGs including carbonyl, epoxide, quinone groups, and the carboxyl armchair edge sites have been regarded as the most active OFGs in different works. This might be caused by the varied structures of carbon matrix such as degree of graphitization, defects, the three-dimensional size, and the presence of heteroatoms, etc. These structure features also influence the local electronic structures to a large extend. Meanwhile, there are usually more than one types of OFGs in oxygen-rich carbon-based catalysts. Therefore, the interactions between different OFGs and the varied structure features make it difficult to evaluate the contribution of specific OFG. Theoretical calculations serve as a powerful tool to screen out the desired structure as well as understand the nature of the electrocatalytic performance of carbon-based electrocatalysts. Notably, nonnegligible gaps may exist between theoretical models and practical materials, which not only makes the results less convincing but also leads to inconsistency between different studies. A major reason is the lack of straightforward approaches to reveal the precise structure of OFGs in oxygen-rich carbon materials. It is rather difficult to observe the structure of carbon matrix and OFGs directly by the scanning transmission electron microscopy (STEM) due to the low contrast of carbon and oxygen atoms. Currently, the characterization of carbon-based materials relies on spectroscopy techniques such as XPS, Raman, FT-IR, and NEXAFS. However, the structures of oxygen-rich carbon materials are usually complex, and the differences between the signals for varied OFGs using these spectroscopy techniques are generally not significant. Therefore, considerable uncertainties may exist in

revealing the structure of OFGs. To address this challenge, future studies may employ highly crystallized graphite or graphene as model materials, which would simplify the materials structure. Also, pyrolyzing oxygen-containing precursors is probably a more feasible method with respect to the precise construction of OFGs, and more efforts should be taken into consideration in future studies. On the other hand, more sophisticated structure models should be considered for theoretical calculation studies in the future. Overall, OFGs play a central role in activating oxygen-rich carbon-based electrocatalysts toward the $2e^-$ ORR, and we believe understanding the nature of OFGs at atomic scale would further enrich the application of oxygen-rich carbon electrocatalysts.

Acknowledgements

This work was financially supported by the National Natural Science Foundation of China (52301293, 52274274), the Natural Science Foundation of Hubei Province (No. 2023AFB584), the "CUG Scholar" Scientific Research Funds at China University of Geosciences (Wuhan) (Project No.2022124) and the Fundamental Research Funds for the Central Universities at China University of Geosciences (Wuhan). G. Zhao acknowledges the financial support from the Natural Science Foundation of Zhejiang province (LQ22B030005).

Received: ((will be filled in by the editorial staff))

Revised: ((will be filled in by the editorial staff))

Published online: ((will be filled in by the editorial staff))

Reference

[1] R. L. Myers, *The 100 most important chemical compounds: a reference guide*, ABC-CLIO, **2007**.

[2] C. Xia, Y. Xia, P. Zhu, L. Fan, H. Wang, *Science* **2019**, 366, 226.

[3] X. Wang, J. Jing, M. Zhou, R. Dewil, *Chin. Chem. Lett.* **2023**, 34, 107621.

[4] Y. Wang, G. I. N. Waterhouse, L. Shang, T. Zhang, *Adv. Energy Mater.* **2021**, 11, 2003323.

[5] X. L. Zhang, X. Su, Y. R. Zheng, S. J. Hu, L. Shi, F. Y. Gao, P. P. Yang, Z. Z. Niu, Z. Z. Wu, S. Qin, *Angew. Chem. Int. Ed.* **2021**, 60, 26922.

[6] Z. Wang, Q.-K. Li, C. Zhang, Z. Cheng, W. Chen, E. A. McHugh, R. A. Carter, B. I. Yakobson, J. M. Tour, *ACS Catal.* **2021**, 11, 2454.

[7] A. A. Ingle, S. Z. Ansari, D. Z. Shende, K. L. Wasewar, A. B. Pandit, *Environ. Sci. Pollut. Res.* **2022**, 29, 86468.

[8] Z. Teng, Q. Zhang, H. Yang, K. Kato, W. Yang, Y.-R. Lu, S. Liu, C. Wang, A. Yamakata, C. Su, B. Liu, T. Ohno, *Nat. Catal.* **2021**, 4, 374.

[9] H. Shin, S. Lee, Y.-E. Sung, *Curr. Opin. Electrochem.* **2023**, 101224.

[10] Y. Jiang, P. Ni, C. Chen, Y. Lu, P. Yang, B. Kong, A. Fisher, X. Wang, *Adv. Energy Mater.* **2018**, 8, 1801909.

[11] S. Anantharaj, S. Pitchaimuthu, S. Noda, *Adv. Colloid Interface Sci.* **2021**, 287, 102331.

[12] N. Wang, S. Ma, P. Zuo, J. Duan, B. Hou, *Adv. Sci.* **2021**, 8, 2100076.

[13] G. O. Santos, P. J. Cordeiro-Junior, I. Sánchez-Montes, R. S. Souto, M. S. Kronka, M. R. Lanza, *Curr. Opin. Electrochem.* **2022**, 101124.

[14] C. Xia, J. Y. Kim, H. Wang, *Nat. Catal.* **2020**, 3, 605.

[15] X. Zhao, Y. Liu, *J. Am. Chem. Soc.* **2021**, 143, 9423.

[16] S. Siahrostami, S. J. Villegas, A. H. Bagherzadeh Mostaghimi, S. Back, A. B. Farimani, H. Wang, K. A. Persson, J. Montoya, *ACS Catal.* **2020**, 10, 7495.

[17] Y. Chen, X. Zheng, J. Cai, G. Zhao, B. Zhang, Z. Luo, G. Wang, H. Pan, W. Sun, *ACS Catal.* **2022**, 12, 7406.

[18] Y. Chen, J. Cai, P. Li, G. Zhao, G. Wang, Y. Jiang, J. Chen, S. X. Dou, H. Pan, W. Sun, *Nano Lett.* **2020**, 20, 6807.

[19] Z. Lu, G. Chen, S. Siahrostami, Z. Chen, K. Liu, J. Xie, L. Liao, T. Wu, D. Lin, Y. Liu, *Nat. Catal.* **2018**, 1, 156.

[20] H. W. Kim, M. B. Ross, N. Kornienko, L. Zhang, J. Guo, P. Yang, B. D. McCloskey, *Nat. Catal.* **2018**, 1, 282.

[21] E. Jung, H. Shin, B.-H. Lee, V. Efremov, S. Lee, H. S. Lee, J. Kim, W. Hooch Antink, S. Park, K.-S. Lee, S.-P. Cho, J. S. Yoo, Y.-E. Sung, T. Hyeon, *Nat. Mater.* **2020**, 19, 436.

[22] H. Zhang, K. Lv, B. Fang, M. C. Forster, R. Dervişoğlu, L. B. Andreas, K. Zhang, S. Chen, *Electrochim. Acta* **2018**, 292, 942.

[23] P. Trogadas, T. F. Fuller, P. Strasser, *Carbon* **2014**, 75, 5.

[24] Y. Bu, Y. Wang, G.-F. Han, Y. Zhao, X. Ge, F. Li, Z. Zhang, Q. Zhong, J.-B. Baek, *Adv. Mater.* **2021**, 33, 2103266.

[25] L. Lin, N. Miao, G. G. Wallace, J. Chen, D. A. Allwood, *Adv. Energy Mater.* **2021**, 11, 2100695.

[26] Y. Zhou, G. Chen, J. Zhang, *J. Mater. Chem. A* **2020**, 8, 20849.

[27] F. Xiang, X. Zhao, J. Yang, N. Li, W. Gong, Y. Liu, A. Burguete-Lopez, Y. Li, X. Niu, A. Fratalocchi, *Adv. Mater.* **2023**, 35, 2208533.

[28] G.-F. Han, F. Li, W. Zou, M. Karamad, J.-P. Jeon, S.-W. Kim, S.-J. Kim, Y. Bu, Z. Fu, Y. Lu, S. Siahrostami, J.-B. Baek, *Nat. Commun.* **2020**, 11, 2209.

[29] I. M. Rocha, O. S. G. P. Soares, J. L. Figueiredo, C. Freire, M. F. R. Pereira, *Catal. Sci. Technol.* **2017**, 7, 1868.

[30] S. Chen, T. Luo, K. Chen, Y. Lin, J. Fu, K. Liu, C. Cai, Q. Wang, H. Li, X. Li, *Angew. Chem.* **2021**, 133, 16743.

[31] Q. Zhang, X. Tan, N. M. Bedford, Z. Han, L. Thomsen, S. Smith, R. Amal, X. Lu, *Nat. Commun.* **2020**, 11, 4181.

[32] K. Lian, Q. Wan, R. Jiang, S. Lin, *Catalysts* **2023**, 13, 307.

[33] M. Mazzucato, C. Durante, *Curr. Opin. Electrochem.* **2022**, 101051.

[34] F. Yang, X. Ma, W.-B. Cai, P. Song, W. Xu, *J. Am. Chem. Soc.* **2019**, 141, 20451.

[35] V. Datsyuk, M. Kalyva, K. Papagelis, J. Parthenios, D. Tasis, A. Siokou, I. Kallitsis, C. Galiotis, *carbon* **2008**, 46, 833.

[36] S. E. Kim, S. K. Jeong, K. T. Park, K.-Y. Lee, H. J. Kim, *Catal. Commun.* **2021**, 148, 106167.

[37] H. Zhang, Y. Li, Y. Zhao, G. Li, F. Zhang, *ACS Appl. Mater. Interfaces* **2019**, 11, 27846.

[38] B. H. R. Suryanto, S. Chen, J. Duan, C. Zhao, *ACS Appl. Mater. Interfaces* **2016**, 8, 35513.

[39] H. Zhao, Z. Tang, M. He, X. Yang, S. Lai, K. An, S. Han, Z. Qu, W. Zhou, Z. Wang, *Sci. Total Environ.* **2023**, 863, 160772.

[40] M.-H. Wang, Q. Li, X. Li, Y. Liu, L.-Z. Fan, *Appl. Surf. Sci.* **2018**, 448, 351.

[41] J. Rodriguez-Zavala, R. Guirado-Lopez, *The Journal of Physical Chemistry A* **2006**, 110, 9459.

[42] B. Li, D. Su, *Chem. Eur. J* **2014**, 20, 7890.

[43] A. J. Plomp, D. S. Su, K. P. d. Jong, J. H. Bitter, *J. Phys. Chem. C* **2009**, 113, 9865.

[44] E. S. Orth, J. G. Ferreira, J. E. Fonsaca, S. F. Blaskievicz, S. H. Domingues, A. Dasgupta, M. Terrones, A. J. Zarbin, *J. Colloid Interface Sci.* **2016**, 467, 239.

[45] A. B. González-Guerrero, E. Mendoza, E. Pellicer, F. Alsina, C. Fernández-Sánchez, L. M. Lechuga, *Chem. Phys. Lett.* **2008**, 462, 256.

[46] C. Pflieger, T. Eckhard, G. Schmitz, V. Angenent, M. Göckeler, O. Senneca, R. Schmid, F. Cerciello, M. Muhler, *ACS Omega* **2022**, 7, 48606.

[47] J. L. Figueiredo, M. Pereira, M. Freitas, J. Orfao, *carbon* **1999**, 37, 1379.

[48] Z. W. Seh, J. Kibsgaard, C. F. Dickens, I. Chorkendorff, J. K. Nørskov, T. F. Jaramillo, *Science* **2017**, 355, eaad4998.

[49] Y. Wang, Y. Zhou, Y. Feng, X.-Y. Yu, *Adv. Funct. Mater.* **2022**, 32, 2110734.

[50] C. Tang, L. Chen, H. Li, L. Li, Y. Jiao, Y. Zheng, H. Xu, K. Davey, S.-Z. Qiao, *J. Am. Chem. Soc.* **2021**, 143, 7819.

[51] W. Wang, Y. Hu, Y. Liu, Z. Zheng, S. Chen, *ACS Appl. Mater. Interfaces* **2018**, 10, 31855.

[52] S. Siahrostami, A. Verdaguer-Casadevall, M. Karamad, D. Deiana, P. Malacrida, B. Wickman, M. Escudero-Escribano, E. A. Paoli, R. Frydendal, T. W. Hansen, *Nat. Mater.* **2013**, 12, 1137.

[53] A. Kulkarni, S. Siahrostami, A. Patel, J. K. Nørskov, *Chem. Rev.* **2018**, 118, 2302.

[54] Y. Guo, R. Zhang, S. Zhang, H. Hong, Y. Zhao, Z. Huang, C. Han, H. Li, C. Zhi, *Energy Environ. Sci.* **2022**, 15, 4167.

[55] C. Zhang, G. Liu, Q. Long, C. Wu, L. Wang, *J. Colloid Interface Sci.* **2022**, 622, 849.

[56] J. Zhu, X. Xiao, K. Zheng, F. Li, G. Ma, H.-C. Yao, X. Wang, Y. Chen, *Carbon* **2019**, 153, 6.

[57] K.-H. Wu, D.-W. Wang, I. R. Gentle, *Carbon* **2015**, 81, 295.

[58] I. Gerber, M. Oubenali, R. Bacsa, J. Durand, A. Gonçalves, M. F. R. Pereira, F. Jolibois, L. Perrin, R. Poteau, P. Serp, *Chem. Eur. J* **2011**, 17, 11467.

[59] F. Avilés, J. V. Cauich-Rodríguez, L. Moo-Tah, A. May-Pat, R. Vargas-Coronado, *Carbon* **2009**, 47, 2970.

[60] U. Cvelbar, B. Markoli, I. Poberaj, A. Zalar, L. Kosec, S. Spaić, *Appl. Surf. Sci.* **2006**, 253, 1861.

[61] X. Fan, W. Peng, Y. Li, X. Li, S. Wang, G. Zhang, F. Zhang, *Adv. Mater.* **2008**, 20, 4490.

[62] C. Qiu, L. Jiang, Y. Gao, L. Sheng, *Materials & Design* **2023**, 230, 111952.

[63] G. Ovejero, J. Sotelo, M. Romero, A. Rodríguez, M. Ocana, G. Rodríguez, J. Garcia, *Ind. Eng. Chem. Res.* **2006**, 45, 2206.

[64] X. Lu, W.-L. Yim, B. H. R. Suryanto, C. Zhao, *J. Am. Chem. Soc.* **2015**, 137, 2901.

[65] R. N. Al-Gaashani, A.Zakaria, Y.Mansour, S.Atieh, M. A., *Ceram. Int.* **2019**, 45.

[66] H. Yu, B. Zhang, C. Bulin, R. Li, R. Xing, *Sci. Rep.* **2016**, 6, 36143.

[67] D. V. Kosynkin, A. L. Higginbotham, A. Sinitskii, J. R. Lomeda, A. Dimiev, B. K. Price, J. M. Tour, *Nature* **2009**, 458, 872.

[68] C. Mattevi, G. Eda, S. Agnoli, S. Miller, K. A. Mkhoyan, O. Celik, D. Mastrogiovanni, G. Granozzi, E. Garfunkel, M. Chhowalla, *Adv. Funct. Mater.* **2009**, 19, 2577.

[69] Y. Wang, M. Yi, K. Wang, S. Song, *Chinese J. Catal.* **2019**, 40, 523.

[70] L. Wang, A. Ambrosi, M. Pumera, *Angew. Chem. Int. Ed.* **2013**, 52, 13818.

[71] J. J. Ternero-Hidalgo, J. M. Rosas, J. Palomo, M. J. Valero-Romero, J. Rodríguez-Mirasol, T. Cordero, *Carbon* **2016**, 101, 409.

[72] S. Kundu, Y. Wang, W. Xia, M. Muhler, *J. Phys. Chem. C* **2008**, 112, 16869.

[73] S. Klink, E. Ventosa, W. Xia, F. La Mantia, M. Muhler, W. Schuhmann, *Electrochem. Commun.* **2012**, 15, 10.

[74] A. Fallah, Y. Nakayama, *Carbon* **2012**, 50, 1879.

[75] S.-J. Park, S.-J. Park, *Composites Part A* **2020**, 137, 105937.

[76] C. H. Choi, H. C. Kwon, S. Yook, H. Shin, H. Kim, M. Choi, *J. Phys. Chem. C* **2014**, 118, 30063.

[77] Z. Shi, J. Zhang, Z.-S. Liu, H. Wang, D. P. Wilkinson, *Electrochim. Acta* **2006**, 51, 1905.

[78] M. Ishifune, R. Suzuki, Y. Mima, K. Uchida, N. Yamashita, S. Kashimura, *Electrochim. Acta* **2005**, 51, 14.

[79] H.-L. Guo, X.-F. Wang, Q.-Y. Qian, F.-B. Wang, X.-H. Xia, *ACS nano* **2009**, 3, 2653.

[80] B. H. R. Suryanto, C. Zhao, *Chem. Commun.* **2016**, 52, 6439.

[81] Z. R. Yue, W. Jiang, L. Wang, S. D. Gardner, C. U. Pittman, *Carbon* **1999**, 37, 1785.

[82] M. Bauer, S. Beratz, K. Ruhland, S. Horn, J. Moosburger-Will, *Appl. Surf. Sci.* **2020**, 506, 144947.

[83] C.-M. Yoon, D. Long, S.-M. Jang, W. Qiao, L. Ling, J. Miyawaki, C.-K. Rhee, I. Mochida, S.-H. Yoon, *Carbon* **2011**, 49, 96.

[84] R. Berenguer, J. P. Marco-Lozar, C. Quijada, D. Cazorla-Amorós, E. Morallón, *Carbon* **2009**, 47, 1018.

[85] T. Gunji, F. Matsumoto, *Inorganics* **2019**, 7, 36.

[86] D. Wang, S. Li, X. Zhang, B. Feng, Y. Pei, Y. Zhu, W. Xu, Z.-H. Li, M. Qiao, B. Zong, *Appl. Catal., B* **2022**, 305, 121036.

[87] W. Xu, Z. Liang, S. Gong, B. Zhang, H. Wang, L. Su, X. Chen, N. Han, Z. Tian, T. Kallio, *ACS Sustainable Chem. Eng.* **2021**, 9, 7120.

[88] C. Wang, D. Wang, S. Zheng, X. Fang, W. Zhang, Y. Tian, H. Lin, H. Lu, L. Jiang, *Chem Res Chin Univ* **2018**, 34, 983.

[89] X. Gan, R. Yuan, J. Zhu, Q. Li, T. Tang, F. Qin, L. Zhu, J. Zhang, L. Wang, S. Zhang, H. Song, D. Jia, *Carbon* **2023**, 201, 381.

[90] H. Zhao, M. Ma, P. Dai, W. Jing, D. Yin, X. Li, H. Xing, W. Ali, N. Ali Khan, P. Li, X. Fan, S. Ding, *Mater. Lett.* **2022**, 322, 132470.

[91] C. Zhang, J. Zhang, J. Zhang, M. Song, X. Huang, W. Liu, M. Xiong, Y. Chen, S. Xia, H. Yang, *ACS Sustainable Chem. Eng.* **2021**, 9, 9369.

[92] J. Zhang, M. Ren, L. Wang, Y. Li, B. I. Yakobson, J. M. Tour, *Adv. Mater.* **2018**, 30, 1707319.

[93] K.-H. Wu, D. Wang, X. Lu, X. Zhang, Z. Xie, Y. Liu, B.-J. Su, J.-M. Chen, D.-S. Su, W. Qi, S. Guo, *Chem* **2020**, 6, 1443.

[94] L. Chu, Z. Sun, L. Cang, X. Wang, G. Fang, J. Gao, *J. Environ. Chem. Eng.* **2023**, 11, 109826.

[95] D. Deng, K. S. Novoselov, Q. Fu, N. Zheng, Z. Tian, X. Bao, *Nat. Nanotechnol.* **2016**, 11, 218.

[96] M. Gonçalves, M. Molina-Sabio, F. Rodriguez-Reinoso, *J. Anal. Appl. Pyrolysis* **2010**, 89, 17.

[97] K. H. Koh, A. H. Bagherzadeh Mostaghimi, Q. Chang, Y. J. Kim, S. Siahrostami, T. H. Han, Z. Chen, *EcoMat* **2023**, 5, e12266.

[98] B. Gong, A. Ikematsu, K. Waki, *Carbon* **2017**, 114, 526.

[99] X. Yang, Y. Zeng, W. Alnoush, Y. Hou, D. Higgins, G. Wu, *Adv. Mater.* **2022**, 34.

[100] Z. Bao, J. Zhao, S. Zhang, L. Ding, X. Peng, G. Wang, Z. Zhao, X. Zhong, Z. Yao, J. Wang, *J. Mater. Chem. A* **2022**, 10, 4749.

[101] X. Lu, X. Zhu, Z. Ma, Z. Che, Y. Li, J. Bao, Y. Liu, *Electrochim. Acta* **2022**, 426, 140755.

[102] X. Wang, N. Li, J. A. Webb, L. D. Pfefferle, G. L. Haller, *Appl. Catal., B* **2010**, 101, 21.

[103] A. Xy, A. Dl, B. Lz, A. Xl, A. Dy, *Appl. Catal., B* **2021**, 304, 120908.

[104] J. S. Lim, J. H. Kim, J. Woo, D. S. Baek, K. Ihm, T. J. Shin, Y. J. Sa, S. H. Joo, *Chem* **2021**, 7, 3114.

[105] E. Zhang, L. Tao, J. An, J. Zhang, L. Meng, X. Zheng, Y. Wang, N. Li, S. Du, J. Zhang, *Angew. Chem.* **2022**, 61.

[106] C. Wan, X. Duan, Y. Huang, *Adv. Energy Mater.* **2020**, 10, 1903815.

[107] X. Zheng, P. Li, S. Dou, W. Sun, H. Pan, D. Wang, Y. Li, *Energy Environ. Sci.* **2021**, 14, 2809.

[108] A. Wang, J. Li, T. Zhang, *Nat. Rev. Chem.* **2018**, 2, 65.

[109] T. Marshall-Roth, N. J. Libretto, A. T. Wrobel, K. J. Anderton, M. L. Pegis, N. D. Ricke, T. V. Voorhis, J. T. Miller, Y. Surendranath, *Nat. Commun.* **2020**, 11, 5283.

[110] Y. Wang, L. Wang, H. Fu, *Sci. China Mater.* **2022**, 65, 1701.

[111] Y. Zheng, P. Wang, W.-H. Huang, C.-L. Chen, Y. Jia, S. Dai, T. Li, Y. Zhao, Y. Qiu, G. I. N. Waterhouse, G. Chen, *Nano Lett.* **2023**, 23, 1100.

[112] H. T. Chung, D. A. Cullen, D. Higgins, B. T. Sneed, E. F. Holby, K. L. More, P. Zelenay, *Science* **2017**, 357, 479.

[113] K. Liu, J. Fu, Y. Lin, T. Luo, G. Ni, H. Li, Z. Lin, M. Liu, *Nat. Commun.* **2022**, 13, 2075.

[114] K. Jiang, S. Back, A. J. Akey, C. Xia, Y. Hu, W. Liang, D. Schaak, E. Stavitski, J. K. Nørskov, S. Siahrostami, H. Wang, *Nat. Commun.* **2019**, 10, 3997.

[115] B.-Q. Li, C.-X. Zhao, J.-N. Liu, Q. Zhang, *Adv. Mater.* **2019**, 31, 1808173.

[116] J. Zhu, S. Mu, *Adv. Funct. Mater.* **2020**, 30, 2001097.

[117] I. D. Rosca, F. Watari, M. Uo, T. Akasaka, *Carbon* **2005**, 43, 3124.

[118] S. Chen, Z. Chen, S. Siahrostami, T. R. Kim, D. Nordlund, D. Sokaras, S. Nowak, J. W. F. To, D. Higgins, R. Sinclair, J. K. Nørskov, T. F. Jaramillo, Z. Bao, *ACS Sustainable Chem. Eng.* **2018**, 6, 311.

[119] X. Tan, H. A. Tahini, S. C. Smith, *Mater. Horizons* **2019**, 6, 1409.

[120] H. W. Kim, H. Park, J. S. Roh, J. E. Shin, T. H. Lee, L. Zhang, Y. H. Cho, H. W. Yoon, V. J. Bukas, J. Guo, H. B. Park, T. H. Han, B. D. McCloskey, *Chem. Mater.* **2019**, 31, 3967.

10.1002/chem.202304065

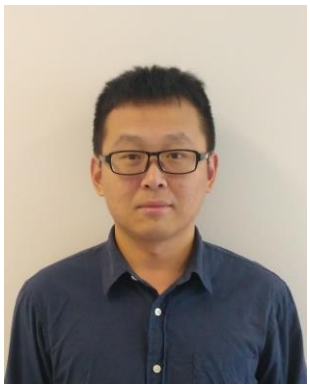

Guoqiang Zhao received his B.S. degree in 2011 from Harbin Engineering University, M.S. degree in 2014 from the Institute of Metal Research, Chinese Academy of Sciences (IMR, CAS), and Ph.D. degree in 2019 from the Institute for Superconducting & Electronic Materials at the University of Wollongong, Australia. He is currently a professor in Engineering Research Center of Nano-Geomaterials of Ministry of Education, China University of Geosciences. His research is focused on developing efficient catalysts for energy conversion reactions.

Huaming Yang is a professor in the Engineering Research Center of Nano-Geomaterials of Ministry of Education at China University of Geosciences, Wuhan, and in the school of Minerals Processing and Bioengineering at Central South University, China. He completed his Ph.D. at Central South University of Technology in 1998, and went to the University of Bristol as a visiting professor from 2008 to 2009. He was awarded the National Science Fund for Distinguished Young Scholars in China. His research interests involve the synthesis strategy and application of energy, environmental and biomedical materials from minerals, and the microstructures of functional materials at the atomic-molecular level.

10.1002/chem.202304065

WILEY-VCH

Oxygen-containing functional groups (OFGs) are crucial in carbon-based electrocatalysts for the two-electron oxygen reduction reaction that enables the flexible synthesis of H_2O_2. Herein, the construction strategies and the specific roles of OFGs are reviewed, aiming to provide inspirations for the future development of advanced carbon-based electrocatalysts for H_2O_2 production.

Guoqiang Zhao,[+] Tianci Chen,[+] Aidong Tang,* Huaming Yang*

Roles of Oxygen-Containing Functional Groups in Carbon for Electrocatalytic Two-Electron Oxygen Reduction Reaction